1

2

3

4

5

Evaluation of the seasonal formation of subsurface negative preformed nitrate

anomalies in the subtropical North Pacific and North Atlantic

8

9

10 Robert T. Letscher[1][*] and Tracy A. Villareal[2]

11

12

13 [1]Earth Sciences and Ocean Process Analysis Laboratory, University of New Hampshire,
14 Durham, NH, USA 03824
15

16 [2]Department of Marine Science and Marine Science Institute, The University of Texas at Austin,

17 Port Aransas, Austin, TX, USA 78382

18

19

20

21 *Correspondance email: robert.letscher@unh.edu

22

23

Abstract

Summertime mixed-layer drawdown of dissolved inorganic carbon in the absence of measurable nutrients in the ocean's subtropical gyres and non-Redfieldian oxygen:nitrate relationships in the underlying subsurface waters are two biogeochemical phenomena that have thus far eluded complete description. Many processes are thought to contribute to one or both including lateral nutrient transport, carbon overconsumption or non-Redfield C:N:P organic matter cycling, heterotrophic nutrient uptake, and the actions of vertically migrating phytoplankton. To obtain insight into the likely magnitude of potential contributing mechanisms that can remove nitrate from the nutricline while supporting dissolved inorganic carbon (DIC) drawdown 10's of meters higher in the water column, we investigated the seasonal formation rates for negative preformed nitrate (preNO$_3$) anomalies (oxygen consumption without stoichiometric nitrate release) in the subsurface and positive preformed nitrate anomalies (oxygen production without stoichiometric nitrate drawdown) in the euphotic zone at the subtropical ocean time series stations ALOHA in the North Pacific and BATS in the North Atlantic. Non-Redfield –O$_2$:N stoichiometry for dissolved organic matter (DOM) remineralization accounts for up to ~15 mmol N m^{-2} yr^{-1} of negative preNO$_3$ anomaly formation at both stations. We present a new formulation for calculating preNO$_3$ (residual preNO$_3$) that includes components resulting from non-Redfield DOM cycling. Residual negative preNO$_3$ anomalies in excess of that which can be accounted for by non-Redfield DOM cycling are found to accumulate at a rate of ~32 – 46 mmol N m^{-2} yr^{-1} at station ALOHA and ~46 – 87 mmol N m^{-2} yr^{-1} at the BATS station. These negative anomaly formation rates are in approximate balance with residual positive preNO$_3$ anomaly formation rates from the euphotic zone located immediately above the nutricline in the water column. We evaluate three mechanisms to explain

47   these anomalies, calculating that transparent exopolymer particles (TEP) cycling and

48   heterotrophic nitrate uptake can contribute to the formation of both residual preNO$_3$ anomalies.

49   However, a significant fraction estimated at ~50 – 95%, is unexplained by the sum of these

50   processes. Vertically migrating phytoplankton possess the necessary distribution, nutrient

51   acquisition strategy and biogeochemical signature to simultaneously remove nitrate at depth and

52   transport it above the nutricline. Reported transport rates by known migrators equal or exceed the

53   residual preNO$_3$ anomaly formation rates and potentially explain both the negative and positive

54   residual preNO$_3$ anomalies as well as the mixed layer DIC drawdown at stations ALOHA and

55   BATS within the limits of scarce detailed abundance profiles. However, the three processes

56   examined are not independent and mutually exclusive. The model *Rhizosolenia* mat system (and

57   perhaps other migrators) produce TEP suggesting that migration could provide accelerated

58   vertical transport of TEP as well as provide labile carbon for heterotrophic nitrate uptake. These

59   results based on geochemical distributions suggest that in the absence of additional mechanisms

60   and rates, phytoplankton vertical migrators, although rare and easily overlooked, play a larger

61   role in subtropical ocean nutrient cycling and the biological pump than generally recognized.

62

63   **Introduction**

64   Subtropical ocean gyre ecosystems exhibit low rates of primary productivity caused by

65   thermal stratification of the water column that acts as an impediment to sustained nutrient supply

66   to the surface ocean. Yet these regions exhibit significant annual net community production

67   (ANCP), estimated at 3 ± 1 mol C m^{-2} yr^{-1} for station ALOHA in the North Pacific (Hawaii

68   Ocean Time-series) and the BATS station (Bermuda Atlantic Time-Series) in the North Atlantic

69   (Emerson, 2014), contributing about half of the global biological carbon pump (Emerson et al.,

70 1997). A seasonal drawdown of mixed layer dissolved inorganic carbon (DIC) occurs at these

71 two well-characterized time-series sites during the summer and early autumn months that is

72 attributed to net community production with minor contributions from lateral mixing and air-sea

73 CO_2 exchange (Gruber et al., 1998, 2002; Keeling et al., 2004; Williams et al., 2013).

74   The nutrient sources supporting this seasonal DIC drawdown at the time-series sites have

75 eluded oceanographers since the phenomenon was first documented (Michaels et al., 1994;

76 Toggweiler, 1994; Gruber et al., 1998; Keeling et al., 2004) and identifying the nutrient sources

77 is essential to understanding how the drawdown occurs. Numerous nutrient input mechanisms

78 have been investigated including vertical mixing, N_2 fixation, atmospheric deposition, and eddy

79 movements with their sum still falling short of explaining the observed DIC drawdown or a

80 stoichiometric equivalent subsurface oxygen consumption (Jenkins and Goldman, 1985; Jenkins

81 and Doney, 2003; Johnson et al, 2010) assuming Redfield stoichiometry between organic matter

82 production and remineralization. More recently, episodic vertical mixing events and lateral

83 advection are two physical mechanisms that have been proposed to supply the surface

84 subtropical gyres with the "missing" nutrients to explain observed ANCP (Johnson et al., 2010;

85 Letscher et al., 2016). However, in order to explain the observed summertime DIC drawdown

86 from the subtropical gyre mixed layer, these two physical mechanisms must supply nutrients,

87 carbon, and oxygen in non-Redfield stoichiometries. Letscher et al. (2016) reported C-deficient,

88 non-Redfieldian supply of inorganic carbon and nutrients within the lateral nutrient streams

89 reaching the subtropical gyres, but this mechanism still falls short of explaining the observed

90 DIC drawdown at stations ALOHA and BATS, even after accounting for non-Redfield C:N:P

91 stoichiometry of organic matter production. Johnson et al. (2010) observed episodic, near

92 monthly, vertical mixing events near station ALOHA that supply nitrate from the nutricline

93   upwards into the euphotic zone to a depth of ~75-100 m. They concluded that the upper 250 m is

94   in approximate balance between nutrient supply and demand and suggested that there are

95   processes that redistribute nitrate within this region. To explain the surface DIC drawdown, these

96   authors suggested the non-Redfieldian supply of nitrate into the mixed layer above ~50 m could

97   be carried out by large, non-flagellated phytoplankton that migrate between the nutricline and the

98   surface as part of their life-history strategy for nutrient acquisition (Villareal et al., 1993; 2014).

99   The oxygen:nitrate distributions in the nutricline provide clues to the possible supply

100   mechanism supporting DIC drawdown. Subtropical gyres exhibit a deficit of sub-euphotic zone

101   nitrate as expected from observed oxygen consumption and Redfield $-O_2{:}N$ organic matter

102   remineralization stoichiometry. This phenomenon is revealed when examining spatiotemporal

103   patterns of the preformed nitrate (preNO$_3$) tracer (all abbreviations are defined in the Appendix,

104   Supplementary Material). preNO$_3$ is traditionally calculated as preNO$_3$ = NO$_{3meas}$ − AOU/R$_{-O2:N}$,

105   where AOU is the apparent oxygen utilization and R$_{-O2:N}$ is the stoichiometric ratio of oxygen

106   consumed to N regenerated for the remineralization of Redfieldian organic matter, e.g. 150:16

107   (Anderson, 1995). preNO$_3$ quantifies the fraction of measured nitrate in a water parcel not

108   attributable to remineralization of Redfieldian organic matter and was initially formulated as a

109   conservative tracer for examining the distribution of water masses involved in the global

110   thermohaline circulation (termed 'NO' by Broecker, 1974). Negative preNO$_3$ (NPN) anomalies

111   occur within upper mesopelagic depths (~100-300 m) of the subtropical ocean, suggesting there

112   are non-Redfieldian processes affecting the *in situ* dissolved oxygen and nitrate pools (Abell et

113   al., 2005; Johnson et al., 2010). That is, the observed negative anomalies are the result of oxygen

114   consumption without concurrent Redfieldian nitrate accumulation. Johnson et al. (2010)

115   suggested that the subsurface NPN anomaly (calculated using a modified Redfield ratio) could

be sustained by vertical separation between nitrate uptake in the nutricline and oxygen

production from net community production near the surface. These authors concluded that

observed mixed layer net community production is mediated by 1) directly observed episodic

vertical physical mixing events that deliver nitrate above 125 m and 2) inferred transport by

vertically migrating phytoplankton transporting this nitrate upwards along a near-zero

concentration gradient within the euphotic zone. Working in the same ecosystem, Ascani et al.

(2013) further reinforced this noting that upper euphotic zone oxygen:nitrate anomalies at station

ALOHA could not be supported by ammonium or DON sources. However, Abell et al. (2005)

approximated non-Redfieldian dissolved organic matter (DOM) cycling and concluded

production, export, and remineralization of DOM with elevated C:N stoichiometry could

quantitatively explain the subsurface preNO$_3$ anomaly distribution in the subtropical North

Pacific.

To date, no work has attempted to partition the contribution of the multiple mechanisms

to formation of the negative preNO$_3$ anomaly and their linkage to DIC drawdown in subtropical

ocean gyres. Multiple lines of evidence indicate that a subset of the oceanic flora is migrating

(Villareal et al., 2014) and transports new nitrogen into the euphotic zone (Villareal et al., 1993;

Richardson et al., 1998; Villareal et al., 1996). Abundance and physiological data require

specialized *in-situ* collections and/or optical enumeration methods (Villareal et al., 2014). As a

result, neither time-series station collects data on this flora. Other hypotheses that have been

advanced to explain the DIC drawdown and/or the subsurface NPN anomaly include

heterotrophic uptake of nitrate and spatially segregated transparent exopolymer (TEP) production

and consumption.

138   In this work, we expand the examination of preNO$_3$ anomalies to the BATS station in the

139   North Atlantic and revisit the missing nutrient and NPN anomaly spatiotemporal distribution at

140   both Station ALOHA and BATS. We build on the approach of Abell et al. (2005) by explicitly

141   calculating the non-Redfield $-O_2$:N remineralization stoichiometry of DOM and incorporating it

142   into the preNO$_3$ equation. This reformulated tracer (residual preNO$_3$) quantifies the preNO$_3$

143   distribution remaining after accounting for non-Redfield $-O_2$:N DOM remineralization

144   stoichiometry. Positive or negative anomalies indicate regions where DOM and particulate

145   organic matter (POM) recycling is unable to explain the residual preNO$_3$ values. Using this new

146   tracer, we identify seasonal formation of a sub-euphotic zone residual negative preNO$_3$ (rNPN)

147   anomaly at the BATS station and a persistent sub-euphotic zone rNPN anomaly at station

148   ALOHA within the nutricline, qualitatively similar to previous results in the subtropical North

149   Pacific using older formulations of preNO$_3$ (Abell et al., 2005; Johnson et al., 2010). In addition,

150   residual positive preNO$_3$ (rPPN) anomalies not previously reported are observed within the

151   euphotic zone (0 – ~80 or ~100 m) at both sites, with integrated rates of formation that are in

152   approximate stoichiometric balance with the rNPN anomalies located immediately below in the

153   water column. These rNPN and rPPN anomalies account for the effects of both POM and DOM

154   remineralization with elevated $-O_2$:N stoichiometry, thus requiring additional mechanisms for

155   their formation. We undertake a quantitative examination of other potential contributing

156   mechanisms to explain the subsurface rNPN anomalies, euphotic zone rPPN anomalies, and

157   mixed layer DIC drawdown including transparent exopolymer particle (TEP) cycling, subsurface

158   bacterial uptake of nitrate, and vertical migration by phytoplankton. We find that TEP cycling

159   may explain a fraction of both the rNPN and rPPN anomalies; bacterial nitrate uptake accounts

160   for only a small fraction of rNPN and none of the rPPN anomalies. In the absence of additional

161   unknown mechanisms, the remaining category (phytoplankton vertical migration) contributes the

162   dominant flux of N to explain both the rNPN (via nitrate consumption and upward transport) and

163   rPPN (via oxygen production during internal nitrate consumption after migration towards the

164   surface) anomalies at both stations ALOHA and BATS. We then compare the calculated

165   requirement to reported rates of nitrate transport by this flora. Distribution maps are provided to

166   highlight the broad distribution of this group and justify comparison of rates from existing

167   datasets to the time-series stations. We hypothesize that nitrate uptake and transport by vertically

168   migrating giant phytoplankton in gyre systems can sustain development of rPPN and rNPN at the

169   two time series stations. In addition, the observed production of TEP by migrating diatom mats

170   (and by inference, other migrators) provides a linkage between at least two of the processes.

171   These calculations provide a framework for evaluating the role of these processes in future

172   studies.

173

174   **Methods**

175   **Data**

176   Time-series biogeochemical data including concentrations of total dissolved nitrogen,

177   nitrate + nitrite, and oxygen for the years 1988-2016 were downloaded from http://bats.bios.edu

178   for the BATS station and http://hahana.soest.hawaii.edu/hot for station ALOHA. Dissolved

179   organic nitrogen (DON) was calculated as total dissolved nitrogen (GF/F 0.7 μm filtered) minus

180   [nitrate + nitrite]. This definition of DON includes ammonium; however, its open ocean

181   concentration is typically < 50 nM and is not regularly measured as part of the two time-series.

182   Global annual climatologies for dissolved O_2 and NO_3^- from the World Ocean Atlas (WOA)

183   2013 (Garcia et al., 2014a; 2014b) were downloaded from http://www.nodc.noaa.gov/OC5. The

184   Global Ocean Data Analysis Project (GLODAP) v2 dataset (Olsen et al. 2016) including

185   dissolved O_2, NO_3^-, CFC-11, and CFC-12 was downloaded from

186   http://www.nodc.noaa.gov/ocads/oceans/GLODAPv2. The WOA and GLODAP data products

187   provide our analysis with an annual time-mean picture of thermocline $preNO_3$ tracer distributions

188   across the larger spatial scales of the North Atlantic, North Pacific, and the other subtropical gyre

189   regions of the global ocean. Water mass ventilation ages on subsurface neutral density layers are

190   computed from the GLODAP v2 CFC-11 and CFC-12 data using a method similar to that

191   described in Doney and Bullister (1992) using the atmospheric time-history of the CFC gases

192   provided by Walker et al. (2000) and the gas solubility constants of Warner and Weiss (1985).

193   All calculations of rNPN and rPPN anomaly formation rates at the time-series sites are

194   performed from analysis of the monthly-resolved station ALOHA and BATS datasets.

195

196   **Tracer computations**

197   The preformed NO_3 tracer defined by Broecker (1974) separates the observationally

198   determined nitrate concentration for a given water parcel into contributions from water mass

199   mixing (preformed) and regenerated from respiration of organic matter. Traditional formulations

200   of $preNO_3$ assign a uniform $-O_2:NO_3$ stoichiometry, e.g. 9.0 (Broecker, 1974), of organic matter

201   remineralization without discriminating between particulate vs. dissolved organic matter (DOM)

202   pools. However, Abell et al. (2005) showed that DOM remineralization stoichiometry is

203   significantly elevated with respect to Redfield proportions in the subtropical North Pacific, with

204    $-O_2:N$ stoichiometries of 23 to 30 within shallow mesopelagic density layers ($\sigma_\theta = 24.4 - 26.1$)

205   compared to Redfield values of 6.9 to 10.6 (Takahashi et al., 1985; Martin et al., 1987; Anderson

206   and Sarmiento, 1994; Paulmier et al., 2009). This required an additional term in the calculation

9

207   of preNO$_3$ in their analysis, accounting for the fraction of oxygen consumption attributable to

208   DOM remineralization and its separate stoichiometry. Abell et al. (2005) inferred the subsurface

209    $-O_2$:N stoichiometry of DOM remineralization from regressions of observed O_2 vs. dissolved

210   organic carbon (DOC) concentrations within upper mesopelagic isopycnal layers. The regression

211   was converted to N units with the separately measured DOC:DON ratio. Here we adopt the Abell

212   et al. (2005) analysis and directly estimate the $-O_2$:N stoichiometry of DON remineralization

213   within upper mesopelagic density layers at stations ALOHA and BATS to compute the residual

214   preNO$_3$ tracer.

215   The residual preNO$_3$ tracer formulation including the effects of DOM remineralization is:

$$residual\ preNO_3 = NO_{3meas} - \left(f_{DOM} \cdot \frac{AOU}{rDOM} \right) - \left(f_{POM} \cdot \frac{AOU}{rPOM} \right) \tag{1}$$

217   NO$_{3meas}$ is the sum of dissolved nitrate + nitrite. Apparent oxygen utilization (AOU) is calculated

218   as AOU $= O_{2sat} - O_{2meas}$; the difference between O_2 saturation at a given temperature, salinity,

219   and pressure with the observationally determined O_2 concentration. The two DOM terms, f_{DOM},

220   the fraction of oxygen consumption attributable to DOM remineralization and r_{DOM}, the

221   stoichiometric ratio of O_2 consumed per mole of DON remineralized, can be determined

222   empirically from the time-series O_2 and DON data. Values of r_{DOM} were determined empirically

223   each year between 1989 – 2000 at station ALOHA and 1993 – 2016 at the BATS station by

224   Model II linear regression (Ricker, 1973; Trujillo-Ortiz and Hernandez-Walls, 2010) of AOU vs.

225   DON within discrete neutral density layers. The subsurface neutral density layers $\gamma^n = 24.2 -$

226   24.7 and $\gamma^n = 24.7 - 25.2$ were chosen at station ALOHA and $\gamma^n = 25.8 - 26.3$ at the BATS

227   station for subsequent calculation of DOM $-O_2$:N remineralization stoichiometry based on a first

228   examination of the depths exhibiting NPN anomalies using the traditional (Redfieldian) preNO$_3$

229   tracer, i.e. preNO$_3 = NO_{3meas} - AOU/R_{-O2:N}$. with the value of R$_{-O2:N}$ selected as 9.0 (Broecker,

230   1974). The fraction of oxygen consumption attributable to DOM remineralization, f_{DOM}, is

231   determined empirically for each neutral density layer following the equation of Abell et al.

232   (2000):

233    $$f_{DOM} = \frac{\Delta DOM}{\Delta DOM + \Delta POM} = \frac{r_{POM}}{r_{DOM}}$$ (2)

234   The stoichiometric ratio of O_2 consumed per mole of particulate organic nitrogen (PON)

235   remineralized, r_{POM}, cannot be uniquely determined from Eq. 2 or the time-series data and is

236   taken from the literature (6.9 to 10.6; Paulmier et al., 2009). We used the climatological average

237   r_{DOM} in Eq. 2 due to a reduced number of years exhibiting statistically significant regressions of

238   AOU vs. DON. Years with a regression correlation coefficient > 0.33 were included in the

239   climatological average (~55% of years investigated). Thus, our approach assumes r_{DOM} and f_{DOM}

240   are constant over time within each density horizon investigated at each station. Relative

241   uncertainty in the literature values of r_{POM} is larger (~55%) than the computed uncertainty in

242   r_{DOM} (~33%). The last remaining term in Eq. 1, f_{POM}, the fraction of AOU attributable to POM

243   remineralization, is calculated as $1 - f_{DOM}$. We tested the sensitivity of our computed residual

244   preNO$_3$ from Eq. 1 and 2 by allowing r_{POM} to vary from 6.9 to 10.6, the upper and lower bound

245   values for r_{POM} reported in the literature (Paulmier et al., 2009).

246   The seasonal formation rate of rNPN anomalies at each time-series site was estimated by

247   a linear regression of the residual preNO$_3$ tracer vs. time within the aforementioned subsurface

248   neutral density layers for the years 1989-2016 at station ALOHA and 1993-2016 at the BATS

249   station. The slope of this regression yields the volumetric rate of rNPN anomaly formation in

250   units of μmol N m^{-3} d^{-1}. The volumetric rates were depth and time integrated to provide annual

251   rates of rNPN anomaly formation in units of mmol N m^{-2} yr^{-1}. Depth integration was performed

252   by estimating the thickness, H, each year of the subsurface neutral density layers of interest at the

253   BATS and ALOHA stations. Values of H varied between 20 to 100 m. Time integration was

254   calculated from the number of days elapsed between the first observation of decreasing residual

255   preNO$_3$ values to the date when residual preNO$_3$ ceased decreasing within the annual cycle (Fig.

256   S1, S2, S4). The volumetric rates of rPPN formation within the euphotic zone and their depth

257   integration at each time-series site were performed within the $0 - 100$ m layer at station ALOHA

258   and within the $0 - 80$ m layer at the BATS station. Time integration for rPPN anomalies was

259   performed analogously to rNPN anomalies; from the time elapsed between observations of

260   increasing residual preNO$_3$ within the euphotic zone over the annual cycle (Fig. S3, S5). For the

261   calculation of the residual preNO$_3$ tracer within the euphotic zone, we made the assumption that

262   the values of f_{DOM} and r_{DOM} were equivalent to those empirically derived for the upper

263   mesopelagic density layer present immediately below the euphotic zone at each site. Seasonal

264   rNPN anomaly formation duration ranged from a minimum of 2 months to a maximum of 10.5

265   months with a median of 7.5 months. Seasonal rPPN anomaly formation duration ranged from a

266   minimum of 4 months to a maximum of 10 months with a median of 6 months.

267   A residual preformed phosphate (prePO$_4$) tracer was computed as:

268
$$residual\ prePO_4 = PO_{4meas} - \left(f_{DOM} \cdot \frac{AOU}{rDOM} \right) - \left(f_{POM} \cdot \frac{AOU}{rPOM} \right) \qquad (3)$$

269   Dissolved organic phosphorus (DOP) concentration data density was not sufficient to allow for

270   statistically significant regressions of AOU versus DOP needed to empirically estimate f_{DOM} and

271   r_{DOM} terms specific to DOP remineralization at each site. To compute prePO$_4$ for each station,

272   we used the values of f_{DOM}, r_{DOM}, and r_{POM} from Table 1 calculated from regressions of AOU vs.

273   DON, converting from N units to P units using a DON:DOP ratio of 16:1 for semilabile DOM

274   remineralization in the subtropical North Atlantic and North Pacific (Letscher & Moore, 2015).

275

Results

DOM remineralization in the upper mesopelagic at the ALOHA and BATS stations

Empirically derived, annual values of r_{DOM} at station ALOHA varied between 10.4 and 24.2 for the $\gamma^n = 24.2 - 24.7$ layer and between 12.7 and 23.5 for the $\gamma^n = 24.7 - 25.2$ layer. Values of r_{DOM} at the BATS station varied between 14.0 and 25.3 in the $\gamma^n = 25.8 - 26.3$ layer. Climatological average r_{DOM} computed for each density layer yielded ratios of 18.1 to 18.9 at station ALOHA and 21.1 at the BATS station (Table 1; standard errors on r_{DOM} are on the order of 33%). These climatological values of r_{DOM} were used in subsequent calculations of residual preNO$_3$ and f_{DOM} from equations 1 and 2. The empirically derived values of r_{DOM} are consistently larger than the literature estimates of r_{POM}, indicating that remineralization of DOM in the upper mesopelagic returns less moles of nitrate per mole of O$_2$ respired at the two sites compared to Redfield stoichiometry.

Empirically derived values of f_{DOM} varied between 0.38 and 0.59 for the $\gamma^n = 24.2 - 24.7$ layer and between 0.36 and 0.6 for the $\gamma^n = 24.7 - 25.2$ layer at station ALOHA. Values of f_{DOM} at the BATS station varied between 0.33 and 0.5 in the $\gamma^n = 25.8 - 26.3$ layer. Climatological average f_{DOM} values of 0.5 for both density layers at station ALOHA and a value of 0.4 at the BATS station (Table 1) were used in subsequent calculation of residual preNO$_3$ from Equation 1.

Upper ocean residual preNO$_3$ climatology at the ALOHA and BATS stations

Station ALOHA – The climatology of the residual preNO$_3$ [μM] tracer is presented for the upper 250 m at station ALOHA in Figure 1a. Residual preNO$_3$ varies between -1 to 1 μM in the upper ~200 m with increasingly positive values below 200 m. The resulting rNPN anomaly (blue colors) is a persistent feature within the 24.2 – 25.2 neutral density layer at a depth of ~100 to

13

299 200 m. Seasonal rPPN anomalies (red colors) are observed immediately above the 24.2 neutral

300 density horizon within the euphotic zone, 0 to ~100 m. Pulses of rPPN anomalies penetrating the

301 bottom of the rNPN anomaly layer are also observed that coincide with shoaling of the 25.2

302 neutral density horizon above 200 m.

303 The monthly averaged climatology of residual $preNO_3$ [μM] at station ALOHA for all

304 data in years 1989 – 2016 is presented in Figure 1b. The subsurface rNPN anomaly is observed

305 to grow in magnitude between the months of May/June through Oct/Nov. There also exists an

306 increase in the magnitude of the rPPN anomaly within the euphotic zone (0 – 100 m),

307 concomitant with the rNPN anomaly formation at ~100 – 200 m depth in summer.

308 Volumetric rates of rNPN anomaly formation at station ALOHA are estimated at 2.8 $\pm$

309 1.4 and 3.0 $\pm$ 1.5 μmol N m^{-3} d^{-1} for the $\gamma^n = 24.2 – 24.7$ layer using r_{POM} values of 6.9 and 10.6,

310 respectively (Table 1). Slightly lower rates of rNPN anomaly formation of 1.6 $\pm$ 0.8 and 2.5 $\pm$

311 1.4 μmol N m^{-3} d^{-1} are estimated for the deeper $\gamma^n = 24.7 – 25.2$ layer at station ALOHA (annual

312 regressions are provided in Fig. S1 & S2). Depth and time integrated, the estimates of rNPN

313 anomaly formation become 28.3 $\pm$ 9.6 (r_{POM} = 6.9) and 17.9 $\pm$ 7.4 (r_{POM} = 10.6) mmol N m^{-2} yr^{-1}

314 for the $\gamma^n = 24.2 – 24.7$ layer and 18.1 $\pm$ 8.8 (r_{POM} = 6.9) and 13.7 $\pm$ 7.8 (r_{POM} = 10.6) mmol N m^{-2} yr^{-1}

315 for the deeper $\gamma^n = 24.7 – 25.2$ layer. Total rNPN formation rate estimates for station

316 ALOHA are between 31.6 $\pm$ 10.8 to 46.4 $\pm$ 13.0 mmol N m^{-2} yr^{-1} (Table 1).

317 The volumetric rate of rPPN anomaly formation within the euphotic zone at station

318 ALOHA is estimated at 3.3 $\pm$ 1.1 and 2.4 $\pm$ 0.8 μmol N m^{-3} d^{-1} using r_{POM} values of 6.9 and 10.6,

319 respectively (Table 1, Fig. S3). These rates are approximately equivalent within error of those

320 estimated for rNPN formation rate within the $\gamma^n = 24.2 – 24.7$ layer immediately below in the

321 water column. Depth and time integrated, the estimate of rPPN anomaly formation is 61.2 $\pm$ 20.2

322   (r_{POM} = 6.9) and 43.5 ± 10.5 (r_{POM} = 10.6) mmol N m^{-2} yr^{-1} (Table 1). The euphotic zone

323   integrated rPPN anomaly is approximately 33% higher than the estimated total integrated rNPN

324   anomaly within the combined γ^n = 24.2 – 25.2 layer.

325   *BATS* – The climatology of the residual $preNO_3$ [µM] tracer in the upper 200 m at BATS

326   is presented in Figure 2a. Residual $preNO_3$ varies between -1 to 1 µM in the upper 200 m and

327   seasonal subsurface rNPN anomalies at ~80 to 160 m depth are observed in most but not all

328   years from 1993 to 2016. Similar to station ALOHA, seasonal pulses of rPPN anomalies are

329   observed immediately above the 25.8 neutral density horizon within the euphotic zone, 0 to ~80

330   m. Pulses of rPPN anomalies penetrating from below the 26.3 neutral density horizon are present

331   in a few years but are much less frequent than observed in the station ALOHA climatology.

332   rPPN anomalies are observed immediately below the rNPN layer beginning at ~160 m.

333   The monthly averaged climatology of residual $preNO_3$ [µM] at BATS for all data in years

334   1993 – 2016 is presented in Figure 2b. The subsurface rNPN anomaly is observed to first appear

335   beginning in Apr/May and grow in magnitude through the end of the calendar year. The rNPN

336   feature starts shallow at a depth of ~60 to 100 m that deepens over the summer months to depths

337   of ~80 to 160 m by years' end. There also exists a layer of rPPN anomaly at 0 – ~80 m depth that

338   increases in magnitude, concomitant with the rNPN anomaly formation at ~80 – 160 m depth in

339   summer and autumn. Late winter convective overturn of the upper water column in late Jan/Feb

340   at the BATS station (Hansell and Carlson, 2001) erases both the subsurface rNPN and 0-80 m

341   rPPN anomaly.

342   The volumetric rate of rNPN anomaly formation at the BATS station is estimated at 5.5 ±

343   2.7 and 3.8 ± 3.1 µmol N m^{-3} d^{-1} for the γ^n = 25.8 – 26.3 layer using r_{POM} values of 6.9 and 10.6,

344   respectively (Table 1, Fig. S4). Depth and time integrated, the estimate of rNPN anomaly

345 formation rate at the BATS station is between 46.0 ± 39.3 to 87.1 ± 41.0 mmol N m^{-2} yr^{-1} (Table

346 1). The volumetric rate of rPPN anomaly formation within the euphotic zone at the BATS station

347 is estimated at 5.8 ± 1.2 and 4.1 ± 0.8 µmol N m^{-3} d^{-1} using r_{POM} values of 6.9 and 10.6,

348 respectively (Table 1, Fig. S5). These rates are approximately equivalent within error of those

349 estimated for rNPN formation rate within the $\gamma^n = 25.8 - 26.3$ layer immediately below in the

350 water column. Depth and time integrated, the estimate of rPPN anomaly formation is 82.1 ± 13.8

351 ($r_{POM} = 6.9$) and 61.8 ± 12.2 ($r_{POM} = 10.6$) mmol N m^{-2} yr^{-1} (Table 1). The euphotic zone

352 integrated rPPN anomaly is approximately balanced ($r_{POM} = 6.9$) or 33% higher ($r_{POM} = 10.6$)

353 than the estimated integrated rNPN anomaly within the $\gamma^n = 25.8 - 26.3$ layer.

354

355 **Upper ocean residual prePO$_4$ climatology at the ALOHA and BATS stations**

356 *Station ALOHA* – The climatology of the residual prePO$_4$ [µM] tracer is presented for the

357 upper 250 m at station ALOHA in Figure 3a. Residual prePO$_4$ varies between -0.04 to 0.2 µM

358 with positive values observed throughout the upper 250 m of the time-series with exception of a

359 period exhibiting small (~0 – -0.04 µM) residual negative prePO$_4$ anomalies at ~125 – 175 m in

360 years 2002 – 2004. The monthly averaged climatology of residual prePO$_4$ [µM] at station

361 ALOHA for all data in years 1989 – 2016 is presented in Figure 3b. Positive residual prePO$_4$ (0 –

362 0.2 µM) is observed throughout the upper 250 m within the monthly averaged climatology.

363 *BATS* – The climatology of the residual prePO$_4$ [µM] tracer in the upper 200 m at BATS

364 is presented in Figure 4a. Residual prePO$_4$ varies between -0.2 to 0.2 µM in the upper 200 m.

365 Seasonal subsurface residual negative prePO$_4$ anomalies at ~80 to 160 m depth are observed in

366 all years from 1993 to 2016 with the exception of 2015. Seasonal pulses of residual positive

367   prePO$_4$ anomalies (~0 – 0.1 µM) are observed immediately above the 25.8 neutral density

368   horizon within the euphotic zone, 0 to ~80 m.

369   The monthly averaged climatology of residual prePO$_4$ [µM] at BATS for all data in years

370   1993 – 2016 is presented in Figure 4b. The subsurface residual prePO$_4$ anomaly is present

371   throughout the seasonal cycle although it is observed to grow in magnitude beginning in May

372   continuing through the end of the calendar year into Jan/Feb, before springtime vertical

373   overturning circulation resets the residual prePO$_4$ concentration in the upper 200 m. The residual

374   negative prePO$_4$ feature starts shallow at a depth of ~80 m in May/Jun that deepens over the

375   summer months to depths of ~80 to 200 m by years' end. There also exists a layer of residual

376   positive prePO$_4$ anomaly at 0 – ~80 m depth that develops during Apr – Nov, concomitant with

377   the seasonally increasing residual negative prePO$_4$ anomaly at ~80 – 200 m depth in summer and

378   autumn.

379

380   **Discussion**

381   Our analysis found DOM remineralization within the upper mesopelagic to follow non-

382   Redfield –O$_2$:N stoichiometry at station ALOHA (~18–19) and the BATS station (~21).

383   However, contrary to the findings of Abell et al. (2005) working in the subtropical North Pacific,

384   this mechanism cannot quantitatively explain the negative preNO$_3$ anomaly present in the

385   subsurface. Instead, we find the euphotic zone to exhibit residual positive preNO$_3$ anomalies and

386   the upper mesopelagic exhibits residual negative preNO$_3$ anomalies at stations ALOHA and

387   BATS. Our directly diagnosed DOM –O$_2$:N remineralization stoichiometry from observations of

388   AOU and DON is significantly lower than that inferred by Abell et al. (2005) (~23–30)

389   diagnosed from AOU vs. DOC remineralization stoichiometry and likely explains this

390   discrepancy. Thus, the fraction of AOU attributable to DOM remineralization and its AOU vs.

391   DON stoichiometry needs to be accounted for in any study that utilizes the preNO$_3$ tracer. The

392   traditional preNO$_3$ tracer calculation should be abandoned and replaced with the residual preNO$_3$

393   tracer formulation as defined in our study (Eq. 1).

394   We now undertake a quantitative examination of the potential contributing mechanisms

395   to explain the subsurface rNPN anomalies and euphotic zone rPPN anomalies.

Physical mechanisms

397   Both the ALOHA and BATS station climatologies of the residual preNO$_3$ tracer exhibit

398   annual cycles of rPPN anomaly formation in the euphotic zone and subsurface rNPN anomaly

399   formation beginning at ~100 m (ALOHA) or ~80 m (BATS) that intensifies from early summer

400   through to mid-autumn (Fig. 1 and 2). This timeframe coincides with the period of thermal

401   stratification of the water column at the BATS station, separating the surface mixed layer, ~0 −

402   30 m, from the deep chlorophyll max (DCM) present at ~100 − 120 m (Navarro and Ruiz, 2013).

403   Station ALOHA exhibits year-round stratification with the DCM present at ~125 m (Navarro and

404   Ruiz, 2013). The largest rPPN anomalies are observed in the vertical zone between the surface

405   mixed layer and the DCM at both sites, at a depth of ~50 − 100 m at station ALOHA and a depth

406   of ~40 − 80 m at the BATS station. This vertical zone of rPPN anomaly formation coincides with

407   the observed subsurface O$_2$ maximum (SOM) that has historically been a conundrum to

408   biogeochemical explanation given the *in situ* ^{14}C-diagnosed net primary production estimates

409   (e.g. Jenkins and Goldman, 1985; Shulenberger and Reid, 1981; Platt et al., 1989). Our rPPN

410   volumetric rates of formation converted to O$_2$ units using the values in Table 1 are approximately

411   20 − 37% (at station ALOHA) of the estimated SOM formation rate in the subtropical central

412   North Pacific and ~34 – 41% (at the BATS station) of the estimated SOM formation rate in the

413   Sargasso Sea (Shulenberger and Reid, 1981).

414   Subsurface rNPN anomalies begin to appear at a depth of ~100 m at station ALOHA and

415   ~80 m at the BATS station continuing down to depths of ~200 m and ~160 m, respectively. We

416   estimated the depth of the top of the nitracline by defining this as the depth where $[NO_3^- + NO_2^-]$

417   = 0.5 μM in the monthly averaged climatologies. At station ALOHA, the top of the nitracline

418   varies between 120 – 130 m depth with a mean of ~126 m over the annual cycle. At the BATS

419   station, the top of the nitracline varies between 90 – 120 m depth with an annual mean of ~102

420   m. Thus, the formation of rNPN anomalies is concurrent with the depth in the water column

421   where nitrate begins to accumulate from remineralization processes at both sites and continues to

422   form deeper into the nitracline.

423   What is the role of lateral physical mixing in creating the observed rPPN and rNPN

424   anomalies? To address this question, we turn to the World Ocean Atlas (WOA) annual O_2 and

425   NO_3^- climatologies (Garcia et al., 2014a; 2014b) on the subsurface isopycnals present in the

426   ~100 – 250 m depth layer at each site. We computed the residual preNO3 tracer for the

427   subtropical North Pacific using the values of f_{DOM} and r_{DOM} for station ALOHA and for the

428   subtropical North Atlantic using the values for the BATS station in Table 1. Examination of the

429   residual preNO3 tracer on the $\gamma^n = 26.5$ density surface (the surface approximately bisecting the

430   150 – 200 m layer near BATS exhibiting rPPN anomalies) reveals that the BATS station is

431   immediately surrounded by waters with a residual preNO3 value of ~1 μM (blue colors; Fig. S6).

432   Waters with a residual preNO3 content of ~2 – 3 μM are present to the southwest and to the

433   northeast (red colors, Fig. S6). The lack of a residual preNO3 gradient on the $\gamma^n = 26.5$ density

434   surface in the immediate vicinity of the BATS station suggests the observed ~1 μM residual

435   preNO₃ concentration present at ~150 – 200 m depth in Figure 2 represents a local signal with

436   little mixing of waters with different residual preNO₃ content. Lateral advective mixing of the

437   higher residual preNO₃ waters to the southwest and northeast of the BATS station would

438   increase the residual preNO₃ on $\gamma^n = 26.5$ to values greater than 1 µM at the BATS station, which

439   is not observed. Plots of residual preNO₃ versus the CFC-11 and CFC-12 age on $\gamma^n = 26.5$ in the

440   North Atlantic reveal essentially no increasing or decreasing residual preNO₃ age gradient (Fig.

441   S6). In summation, this evidence suggests the BATS station sits within the NW corner of a large

442   region of the subtropical North Atlantic characterized by a residual preNO₃ content of ~1 µM on

443    $\gamma^n = 26.5$ that is generated within the basin.

444   On the $\gamma^n = 26.0$ isopycnal which bisects the layer exhibiting the rNPN anomaly at the

445   BATS station, the site sits surrounded by waters with a residual preNO₃ content of ~0 µM in the

446   annual climatology, with more distant waters exhibiting rNPN anomalies south of ~27 ºN and

447   waters with rPPN anomalies north of ~37 ºN (Fig. S7). Plots of residual preNO₃ versus CFC-11

448   and CFC-12 age on $\gamma^n = 26.0$ again reveal essentially no residual preNO₃ gradient with

449   increasing age (Fig. S7). Given the lack of a residual preNO₃ tracer gradient with water mass age

450   and the observation of a repeating seasonal pattern of rNPN anomaly formation at the BATS

451   station on $\gamma^n = 26.0$ (Fig. 2), we conclude that lateral advective mixing cannot explain the

452   observed seasonal rNPN anomalies, instead suggestive of biological mechanisms supporting

453   rNPN anomaly formation at the BATS station.

454   Examination of the residual preNO₃ tracer on the $\gamma^n = 25.4$ density surface (the surface

455   approximately bisecting the 200 – 250 m layer near ALOHA) in the North Pacific within the

456   WOA climatology reveals that station ALOHA sits near the southern boundary of waters with a

457   residual preNO₃ content of 0 – 1.5 µM that extends as far north as 40 ºN and as far east as 130

458   ºW (Fig. S8). Waters with higher residual preNO$_3$ content of 2 – 4 µM are located to the south of

459   station ALOHA, beginning around the vicinity of the big island of Hawaii (Fig. S8).

460   Examination of plots of residual preNO$_3$ versus CFC-11 and CFC-12 age on $\gamma^n = 25.4$ in the

461   North Pacific reveals that station ALOHA lies between younger, low residual preNO$_3$ content

462   waters to the north with older, higher residual preNO$_3$ content waters to the south (Fig. S8).

463   Mixing of these waters along $\gamma^n = 25.4$ may explain the observed ~1 µM residual preNO$_3$

464   concentration present at 200 – 250 m depth in Figure 1. This feature is noticeably absent at

465   BATS, (Figure S6) consistent with a minor role for advective mixing there.

466   On the $\gamma^n = 24.7$ isopycnal which bisects the density layer exhibiting the rNPN anomaly

467   at station ALOHA, the site is surrounded by waters with rNPN anomalies on the order of $-1 - 0$

468   µM (Fig. S9). Plots of residual preNO$_3$ versus CFC-11 and CFC-12 age on $\gamma^n = 24.7$ reveal

469   essentially no residual preNO$_3$ age gradient (Fig. S9). Similar to the BATS station, given the lack

470   of a residual preNO$_3$ age gradient on $\gamma^n = 24.7$ and the observation of seasonal formation of

471   rNPN anomalies, we conclude that lateral advective mixing cannot explain the observed rNPN

472   anomalies, suggestive of biological mechanisms.

473   **Biological mechanisms**

474   Lateral mixing may explain the observed rPPN anomaly below ~200 m at station

475   ALOHA: however, the euphotic zone rPPN anomalies and subsurface rNPN anomalies at each

476   site are generated by a local biological mechanism. Biological formation of rNPN anomalies

477   requires either O$_2$ consumption without concomitant stoichiometric nitrate accumulation or

478   nitrate drawdown without concomitant stoichiometric O$_2$ production. Formation of rPPN

479   anomalies requires either O$_2$ production without concomitant stoichiometric nitrate drawdown or

480   nitrate accumulation without concomitant stoichiometric O$_2$ consumption. Having accounted for

481 the non-Redfield $-O_2$:N DOM remineralization stoichiometry at each site (see Table 2 for the

482 rate of NPN/PPN anomaly formation attributable to N-poor DOM remineralization), we

483 hypothesize three other biological mechanisms to explain the observed seasonal formation rates

484 and integrated quantities of concurrent rPPN accumulation in the euphotic zone and rNPN

485 accumulation in the subsurface at the ALOHA and BATS stations: 1) vertically separated

486 biological production, export, and remineralization of N-deficient transparent exopolymer

487 particles (TEP); 2) heterotrophic bacterial uptake of nitrate to remineralize N-poor organic

488 matter; 3) vertical migration of autotrophic phytoplankton down to the nutricline to acquire

489 nitrate with subsequent photosynthetic oxygen production within the euphotic zone.

490 *TEP* – Transparent exopolymer particles (TEP) are the polysaccharide-rich exudate of

491 phytoplankton that accumulate in the size range <1 to >100 μm in aquatic systems (Mari et al.,

492 2017). TEP is both sticky and positively buoyant in seawater (Azetsu-Scotte and Passow, 2004),

493 leading to aggregation and flotation towards the surface, with large enrichments of TEP present

494 in the sea surface microlayer (Wurl et al., 2009). Being comprised of nearly pure saccharide

495 material, TEP is a carbon rich and essentially N-deficient pool of non-sinking particulate organic

496 carbon formed within the euphotic zone of marine systems by phytoplankton production

497 (Alldredge et al., 1993). TEP production has been hypothesized to contribute to "carbon

498 overconsumption" in low nutrient oligotrophic marine ecosystems (Toggweiler, 1993) where

499 organic matter is produced in non-Redfield, C-rich/N-poor proportions. Due to its positive

500 buoyancy (Mari et al., 2017), TEP has been viewed as a non-contributor to upper ocean carbon

501 export; however, some portion of the TEP pool is associated with sufficient ballasting particles

502 (e.g. clays, biogenic minerals) to achieve negative buoyancy, and may comprise a slowly sinking

503 (a few meters per year) pool of organic carbon exported below the euphotic zone (Mari et al.,

504   2017). TEP production and remineralization stoichiometry has the correct sense; O_2 production

505   without Redfieldian nitrate drawdown within the euphotic zone, O_2 consumption without

506   Redfieldian nitrate accumulation within the mesopelagic, to contribute to both the observed

507   rPPN anomalies within the euphotic zone and rNPN anomalies in the upper mesopelagic at the

508   ALOHA and BATS stations.

509   We use field data of TEP concentrations near the BATS and ALOHA stations and a few

510   simplifying assumptions to test for the importance of this process as a contributor to the dual

511   rNPN/rPPN anomalies. Our estimates of the potential for TEP cycling to contribute to the

512   observed euphotic zone rPPN and subsurface rNPN anomaly formation rates assume 1) that TEP

513   is pure carbohydrate (CH_2O); without any N content, such that TEP production/remineralization

514    $C:O_2$ stoichiometry can be assumed 1:1 (e.g. $CO_2 + H_2O \Leftrightarrow CH_2O + O_2$), and 2) that there exists

515   a sufficiently large and dense TEP pool to sink rapidly enough to contribute to annual carbon

516   export and O_2 remineralization budgets. Both assumptions, if incorrect, will overestimate the

517   TEP contribution. In conjunction with TEP cycling, Coomassie stainable particles are transparent

518   protein-containing particles (Long and Azam, 1996) that can reach similar concentrations within

519   the oligotrophic euphotic zone as TEP (Cisternas-Novoa et al., 2015). Thus, the assumption that

520   transparent exopolymer particle cycling delivers only C to the subsurface to drive rNPN anomaly

521   formation may not be entirely valid. In addition, Mari et al. (2017) note that elevated TEP

522   concentrations likely enhance material retention in the euphotic zone. Thus, our calculations that

523   follow tend to maximize the contribution of TEP.

524   Cisternas-Novoa et al. (2015) measured TEP concentration depth profiles in the Sargasso

525   Sea northeast of Bermuda on five separate occasions from February 2012 to June 2013. The

526   profiles show a ~10 µg XG eq L^{-1} (xanthum gum equivalent) concentration excess between the

23

527   upper 100 m and the 100-200 m layer (Fig. 15 in Cisternas-Novoa et al., 2015). We take this

528   upper 100 m excess to represent the fraction of the euphotic zone TEP pool that is exported

529   annually to the upper mesopelagic 100-200 m depth layer by a combination of physical sinking

530   of a fraction of the TEP pool that becomes negatively buoyant or is delivered to the subsurface

531   with wintertime vertical mixing. This assumption is supported by the observation that the

532   euphotic zone to mesopelagic TEP concentration gradient is nearly erased in the winter profile,

533   presumably due to wintertime convective mixing, and reappears following the spring bloom,

534   remaining relatively unchanged throughout the late spring/summer month profiles. TEP in

535   xanthum gum equivalents can be converted to μg C L^{-1} units using a 0.63 conversion factor

536   (Engel, 2004) and again into μM units, yielding a Sargasso Sea upper ocean concentration excess

537   of ~0.5 μM TEP-C. Integrating over the surface to 80 m depth layer (the depth where rPPN

538   anomalies switch to rNPN anomalies), we obtain a potential TEP production and export flux of

539   42 mmol TEP-C m^{-2} yr^{-1} from the euphotic zone into the upper mesopelagic. Assuming 1:1 $C:O_2$

540   TEP production/remineralization stoichiometry, an O_2 production flux in the absence of nitrate

541   drawdown of 42 mmol O_2 m^{-2} yr^{-1} can be ascribed to TEP production within the euphotic zone,

542   and the same flux can be ascribed to O_2 consumption without concomitant nitrate accumulation

543   from TEP remineralization in the mesopelagic. We can convert this O_2 flux to a residual $preNO_3$

544   equivalent using Equation 1 and the values in Table 1, yielding estimates of 3.2 – 4.5 mmol N m^{-2}

545   ^{2} yr^{-1} residual $preNO_3$ anomaly formation rate equivalents, depending on the choice of r_{POM}.

546   Thus, TEP formation within the euphotic zone of the Sargasso Sea has the potential to explain

547   5.2 – 5.4% of the estimated rPPN anomaly formation rate and 5.1 – 7.0% of the estimated rNPN

548   anomaly formation rate within the $\gamma^n = 25.8 – 26.3$ layer (Table 2).

549   The potential contribution of TEP cycling to rPPN/rNPN anomaly formation near the

550   BATS station can be also be estimated using published sinking rates for negatively buoyant TEP.

551   Again, using the TEP profiles from the Sargasso Sea from Cisternas-Novoa et al. (2015), we

552   estimate a concentration difference of ~5 μg XG eq L^{-1} between 100 m and 200 m depth (the

553   approximate depths exhibiting rNPN anomalies). Converting to molar carbon concentration

554   yields a quantity of ~0.26 μM TEP-C that is apparently remineralized within the rNPN anomaly

555   layer. We apply the TEP sinking rate of 0.04 d^{-1} from Hamanaka et al. (2002) to estimate the rate

556   of delivery of exported TEP from the euphotic zone into the upper mesopelagic, yielding a TEP

557   supply and remineralization flux of 10 μmol C m^{-3} d^{-1}. Depth and time integrated to 15 meters

558   and one year, i.e. the depth slowly sinking TEP will sink after one year, this flux becomes 56.9

559   mmol C m^{-2} yr^{-1} or O_2 units assuming 1:1 $C:O_2$ stoichiometry for TEP. Conversion of this O_2

560   flux into residual $preNO_3$ equivalents yields an estimated 4.3 – 6.0 mmol N m^{-2} yr^{-1} of the

561   observed rPPN/rNPN anomaly formation rate attributable to TEP cycling. Thus, computed using

562   the sinking rate, TEP formation within the euphotic zone has the potential to explain 7.0 – 7.3%

563   of the estimated rPPN anomaly formation rate and 6.9 – 9.3% of the estimated rNPN anomaly

564   formation rate within the $\gamma^n = 25.8 – 26.3$ layer.

565   Seasonal depth profiles of TEP concentration are unavailable for the subtropical North

566   Pacific near station ALOHA. Wurl et al. (2011) measured TEP concentration profiles south of

567   the island of Hawaii during August/September 2009. We use the upper ocean concentration

568   excess present in these profiles with the TEP sinking rate of 0.04 d^{-1} to estimate the TEP cycling

569   contribution to rPPN/rNPN anomaly formation rates near station ALOHA. The 100 to 200 m

570   concentration excess in TEP-C is ~1 μM yielding an export and supply flux of 40 μmol C m^{-3} d^{-}

571   ^{1}. Depth and time integrating for 15 m and one year, this flux becomes 220 mmol C m^{-2} yr^{-1}

572   (mmol O_2 m^{-2} yr^{-1}). Conversion of this O_2 flux to residual preNO$_3$ equivalents using equation 1

573   and values in Table 1, yields an estimated $16.2 - 21.8$ mmol N m^{-2} yr^{-1} of the observed

574   rPPN/rNPN anomaly formation rate potentially attributable to TEP cycling at station ALOHA.

575   Thus, TEP formation within the euphotic zone has the potential to explain $35.6 - 37.2\%$ of the

576   estimated rPPN anomaly formation rate and $47.0 - 51.3\%$ of the total estimated rNPN anomaly

577   formation rate within the combined $\gamma^n = 24.2 - 25.2$ layer (Table 2).

578   *Bacterial nitrate uptake* – Multiple studies have shown the uptake of nitrate and/or

579   phosphate by heterotrophic bacteria during the remineralization of organic matter or that

580   inorganic nutrients can limit bacterial OM consumption (e.g. Zweifel et al., 1993; Kirchman,

581   1994; Cotner et al., 1997; Rivkin and Anderson, 1997; Caron et al., 2000; Letscher et al., 2015).

582   Bacterial nitrate uptake to remineralize OM has the effect of creating an NPN anomaly (O_2

583   consumption without concomitant nitrate accumulation) and thus can only contribute to the

584   observed subsurface rNPN anomaly formation. It cannot contribute to either the formation of the

585   euphotic zone rPPN anomaly or surface mixed layer drawdown of DIC. If TEP cycling is an

586   important contributor to oligotrophic ocean C export and shallow subsurface O_2 consumption,

587   heterotrophic bacterial nitrate and/or phosphate uptake is a likely complementary biological

588   process, since the nutrient deficient content of TEP could require exogenous uptake of N and P

589   from the seawater media for bacterial production when growing on TEP organic matter. This

590   would result in an imbalance between rPPN and rNPN, in contrast to the results presented

591   earlier.

592   To assess the potential contribution of bacterial nitrate uptake to our observed rNPN

593   anomaly formation rates at the ALOHA and BATS stations, we examined the literature for

594   estimates of bacterial C production rates and bacterial biomass C:N ratios for the Sargasso Sea

595   and subtropical North Pacific. Carlson et al. (1996) measured bacterial production rates at the

596   BATS station using the ^{3}H-thymidine and ^{3}H-leucine uptake methods with average euphotic

597   zone rates of 23 pmol C L^{-1} d^{-1} by ^{3}H-thymidine and 0.41 nmol C L^{-1} d^{-1} by ^{3}H-leucine. Using a

598   bacterial biomass C:N of 5:1 for this region (Gunderson et al. 2002) and integrating for one year

599   and over the ~80 – 160 m thick layer exhibiting rNPN anomaly, yields an estimate of 0.17 – 3.0

600   mmol N m^{-2} yr^{-1} bacterial N demand. If we assume that bacteria satisfy *all* of their N demand via

601   uptake of seawater nitrate in this shallow subsurface layer, bacterial nitrate uptake can explain at

602   most 0.5 – 3.5% of the estimated rNPN anomaly formation rate at the BATS station in the γ^n =

603   25.8 – 26.3 layer. This proposed mechanism still requires a process that removes bacterial N

604   from the γ^n = 25.8 – 26.3 layer such that a rNPN anomaly is observed due to NO_3 uptake in the

605   absence of stoichiometric O_2 accumulation. Diel vertically migrating grazers are a candidate

606   mechanism whereby grazing on bacterial biomass and its eventual remineralization to NO_3 is

607   spatially separated from respiration and O_2 consumption.

608   We can make a similar calculation for station ALOHA using published ^{3}H-leucine

609   bacterial production rate measurements (Church et al., 2004). The mean bacterial C production

610   rate at 100 m is ~0.46 nmol C L^{-1} d^{-1}. Using the same bacterial biomass C:N of 5:1 and

611   integrating for one year over the ~100 – 200 m thick layer exhibiting rNPN anomaly, yields an

612   estimated 3.4 mmol N m^{-2} yr^{-1} bacterial N demand. If we again assume that bacteria satisfy *all* of

613   their N demand from nitrate uptake, this process can explain at most 0 – 7% of the estimated

614   rNPN anomaly formation rate at station ALOHA in the combined γ^n = 24.2 – 25.2 layer.

615   *Vertically migrating phytoplankton* – From our analyses of the available published data,

616   neither remineralization of N-poor DOM, TEP cycling, or heterotrophic bacterial nitrate uptake

617   can quantitatively explain both the seasonal rPPN anomaly formation within the euphotic zone

618 and subsurface rNPN anomaly formation observed at the ALOHA and BATS stations, even with

619 the generous assumptions made. We now examine the vertical migration of phytoplankton down

620 to the nutricline as a potential biological mechanism to explain the dual rPPN/rNPN anomalies.

621 In the absence of other mechanisms, the potential contribution of vertically migrating

622 phytoplankton to the rNPN and rPPN anomaly features at the two stations can be determined by

623 subtracting the contributions of TEP cycling and bacterial nitrate uptake to rNPN and/or rPPN

624 formation from the total observed rNPN/rPPN anomaly formation rates (presented in Table 2).

625 By difference, the phytoplankton vertical migration category must provide $16 - 21$ mmol N m^{-2}

626 yr^{-1} or $45 - 50\%$ of rNPN anomaly formation and $27 - 36$ mmol N m^{-2} yr^{-1} or $59 - 62\%$ of rPPN

627 anomaly formation at station ALOHA (Table 2). At the BATS station, phytoplankton vertical

628 migration must provide $43 - 78$ mmol N m^{-2} yr^{-1} or $90 - 93\%$ of rNPN anomaly formation and

629 $59 - 76$ mmol N m^{-2} yr^{-1} or $87 - 95\%$ of rPPN anomaly formation. These are likely

630 underestimates because the bacterial nitrate uptake and TEP contribution are maximum

631 estimates.

632 As a rare, giant component of the flora, net collections, *in-situ* observations by divers,

633 and towed optical systems constitute the bulk of observations; hence vertical migrators are

634 somewhat out of the mainstream of current phytoplankton observations. The unique attributes

635 and evidence for vertical migration are briefly discussed here for background, as well as

636 documentation of their presence in both oceans at or near the time-series stations. Nitrate

637 transport rates are then summarized for comparison to the required contribution from the residual

638 preNO$_3$ anomaly flux budgets.

639 Flagellate motility and cyanobacteria buoyancy control has been recognized for decades

640 as a strategy to exploit spatially disjunct light and nutrient fields (Cullen, 1985; Eppley et al.,

641 1968, Ganf and Oliver, 1982; Hasle, 1950; Steemann Nielsen, 1939) and was suggested for non-

642 flagellated marine species in *Pyrocystis* (Sukhanova and Rudyakov, 1973; Ballek and Swift,

643 1986; Rivkin et al., 1984). *Rhizosolenia* mats (macroscopic, multi-species (up to 7) associations

644 of *Rhizosolenia* spp.; Villareal and Carpenter, 1989) have been the model for understanding this

645 process (Villareal et al., 2014), with migration inferred for the diatoms *Ethmodiscus* spp. and

646 large *Rhizosolenia* spp., as well as the phycomate prasinophyte *Halosphaera* spp. in addition to

647 *Pyrocystis.* There is consistent evidence of high $\delta^{15}N$ composition of *Rhizosolenia* biomass

648 similar to sub-nitracline N (Villareal et al., 1993, Villareal et al., 2014), internal millimolar

649 nitrate pools that can only be acquired by direct uptake at μM concentrations (Villareal and

650 Lipschultz, 1995; Villareal et al., 1996; Woods and Villareal, 2008), buoyancy reversals linked

651 to nutrient status (Richardson et al., 1996), nitrate reductase activity (Joseph et al., 1997) induced

652 only when nitrate is the primary N source, ascent/descent rates of multiple m hr^{-1} (Villareal et al.,

653 2014; Moore and Villareal 1996), observation of *Rhizosolenia* mats from the surface to 305 m

654 (Pilskaln et al., 2005), and compositional difference in floating and sinking mats that mirror

655 physiological changes associated with nutrient depletion and carbohydrate ballasting (Villareal et

656 al., 1996). A key attribute in all giant phytoplankton (10^{7+} μm^3) migrators is multiple m hr^{-1}

657 ascent/descent rates that permit 50–100 m vertical excursions (Moore and Villareal, 1986). This

658 large vacuole of these giant phytoplankton allows the necessary storage (mM concentrations in

659 vacuoles that are 90+% of total cell volume) for a multiple day migration and division cycle.

660 Unlike the more widely known zooplankton vertical migration, open ocean phytoplankton

661 migration is a multi-day cycle (Richardson et al., 1998; Villareal et al., 1996). It is asynchronous

662 and not cued to diel rhythms as in coastal dinoflagellates or vertically migrating zooplankton.

663   Giant phytoplankton are found throughout the warmer oceans of the world and are

664   specifically noted at both stations ALOHA and BATS (Figure S11-13). The required

665   characteristics of buoyancy reversals, high internal nitrate pools and rapid ascent/descent have

666   been found in multiple taxa from the Atlantic and Pacific Oceans (Villareal et al., 2014). The

667   taxa *Halosphaera* (Villareal and Lipschultz, 1995), *Ethmodiscus* (Villareal and Lipschultz,

668   1995), *Rhizosolenia* (Villareal and Lipschultz, 1995), and *Pyrocystis* (Swift et al. 1973, Rivkin et

669   al 1984, Villareal and Lipschultz 19965) occur in the Sargasso Sea and all exhibit positive

670   buoyancy and have mM internal nitrate pools. In the Sargasso Sea, the non-motile dinoflagellate

671   *Pyrocystis* has been the most extensively studied by E.J. Swift's lab in the 1980s. A 'once in a

672   generation' migration cycle (Sukhanova and Rudyakov, 1973) was proposed for *Pyrocystis*

673   based on differences in vegetative and reproductive cell maxima (~60 and 120 m, respectively).

674   Vegetative stages were positively buoyant (up to 0.2 m h^{-1}; Kahn and Swift, 1978) while

675   reproductive stages were negatively buoyant at up to 18 m h^{-1} in the Mona Passage, southwest N.

676   Atlantic (Swift et al. 1976). In the Sargasso Sea, carbon budgets (Rivkin et al., 1984) and

677   buoyancy changes upon nutrient depletion and addition (Ballek et al., 1986) all supported a

678   vertical migration life cycle. In single-cell analysis from field material collected off Bermuda,

679   *Pyrocystis* internal nitrate concentrations ranged from 0-8 mM with floating cells containing

680   significantly higher concentrations (*p*=0.05) than sinking cells (Villareal and Lipschultz, 1995).

681   Such elevated internal nitrate can only be acquired at μM nitrate concentrations found in the

682   nutricline. Abundance maxima in the upper ~200 m of the Sargasso Sea/southwest N. Atlantic

683   range from 100-200 cells m^{-3}, with typical values reported of 18-75 cells m^{-3} (Rivkin et al.,

684   1984), 10-50 cells m^{-3} (Ballek and Swift, 1986) and 10-30 cells m^{-3} (Swift et al., 1981). While

685   the other migrating taxa are found in the Sargasso Sea near Bermuda, there is no data on

686   abundance in the N. Atlantic other than for *Ethmodiscus*. *Ethmodiscus* was found at every station

687   sampled on three cruises in the southwest N. Atlantic (n=18, ~17-25°N, 66-77°W) with

688   abundance ranging from 0.03-4.7 cells m^{-3}. Free-living chains of *Rhizosolenia* were routinely

689   isolated by hand-collection with SCUBA at Bermuda (Moore and Villareal, 1996a,b; Richardson

690   et al., 1996) and were widely noted by Carpenter et al. (1977) in the Caribbean. Cleve (1900)

691   reported *R. castracanei* (a giant, migrating diatom found both free-living and in *Rhizosolenia*

692   mats) to occur in the Sargasso Sea as well as the tropical Atlantic, Caribbean Sea, Florida current

693   to Newfoundland Banks, and the Azores.

694   In the Pacific, the range of *Ethmodiscus*, *Pyrocystis*, and *Rhizosolenia* mats includes the

695   study site at station ALOHA (Figures S11-13). Unlike the Atlantic where mats are generally very

696   rare (~0.001 mats m^{-3}, Carpenter et al., 1977), *Rhizosolenia* mats dominate in the Pacific.

697   Abundance ranges up to several hundred mats m^{-3}, depending on the mat size and enumeration

698   methods (Villareal et al., 1996, Villareal et al., 1999; Villareal et al., 2014). Quantitative net

699   surveys of *Ethmodiscus* north of Hawaii yielded abundance ranges of <0.1 – >2 cells m^{-3}

700   (Villareal et al., 2007). Both *Halosphaera* and *Pyrocystis* were present, but not quantified.

701   Further to the west, Soviet-era literature documents *Pyrocystis* at 10-50 cells m^{-3} in the upper 200

702   m (Sukhanova and Rudyakov, 1973; Sukahova, 1973). Free-living giant *Rhizosolenia* were

703   observed by divers at all stations sampled in the N. Pacific (Villareal, unpubl. obs.), and

704   overlapped 100% with *Rhizosolenia* mats (Fig. 2 in Villareal et al., 2014); *R. castracanei* was

705   reported across the Pacific Ocean (Fig. 8 in Semina and Levashova, 1977). It should be noted

706   that net collections disrupt *Rhizosolenia* mats (Alldredge and Silver, 1982) and the large

707   diameter species such as *R. castracanei* in the mats will appear as free-chains and cells in the

708   literature.

709   For rNPN and rPPN development, the unique characteristics of vertical migration are that

710   cells acquire and store nitrate at depth, transport it into the euphotic zone, and then reduce it

711   internally to biomass concomitant with oxygenic photosynthesis. Nitrate transport calculations

712   by vertical migration have a number of assumptions and caveats including variability in

713   abundance, particularly for *Halosphaera* spp. (Villareal et al., 2014). Inclusion of small-sized

714   *Rhizosolenia* mats missed by divers (Villareal et al. 1999) in estimates yielded rates of 6–444

715   μmol N m^{-2} d^{-1} (mean = 171 ± std. dev.187 μmol N m^{-2} d^{-1}) at four stations north of station

716   ALOHA. Assuming a 180 day production period, this converts to $1.1 - 80$ mmol N m^{-2} y^{1} (mean

717     $= 30 \pm$ std. dev. 34 mmol N m^{-2} y^{-1}. Using a generalized gyre abundance (Villareal et al. 2014),

718   four other taxa yielded transport rates of 3.2 (*Ethmodiscus* spp.), 9.2 (free living *Rhizosolenia*

719   spp.), 17.0 (*Pyrocystis* spp.) and 33.2 (*Halosphaera* spp.) μmol N m^{-2} d^{-1} for a total of 62.5 μmol

720   N m^{-2} d^{-1} (11.2 mmol N m^{-2} y^{-1}). These taxa exhibit basin-specific abundance patterns (i.e.

721   *Rhizosolenia* mats are rare in the N. Atlantic; Carpenter et al., 1977, *Halosphaera viridis* has an

722   extensive subsurface presence in the deep Mediterranean in winter (Wiebe et al., 1974)), but the

723   generalized abundance and distribution data are consistent with required rNPN and rPPN rates at

724   both the BATS station (43-78 and 59-76 μmol N m^{-2} d^{-1}, respectively) and station ALOHA (16-

725   21 and 27-36 μmol N m^{-2} d^{-1}, respectively). *Rhizosolenia* mats alone may be sufficient to support

726   rNPN and rPPN rates at station ALOHA. There are several implications of this. Lower

727   abundance or turnover times of this flora will still have substantial effects on rNPN and rPPN.

728   Patchiness in abundance (Villareal, 2007; Villareal et al., 2014) or concentration of buoyant

729   particles by mesoscale fronts (Guidi, 2012) could lead to significant local perturbations on rNPN

730   and rPPN.

731   Fraga (2001) developed an independent assessment of the impact of vertical migration on

732   the NO tracer (functionally related to our residual preNO$_3$ tracer) based on first principles of

733   photosynthetic production and biosynthesis of biomass. For ecosystems containing both coastal

734   dinoflagellates and oceanic diatoms, a subsurface minimum in NO and a related tracer, NCO

735   (NO corrected for the stoichiometry of carbohydrate synthesis) formed. For migrating

736   *Rhizosolenia*, the NO and NCO minimum was at ~150 m with negative anomalies from ~80 to

737   ~200 m (Fig. 6 in Fraga, 2001). The Fraga (2001) formulation also included an explicit term for

738   release of soluble carbohydrate (functionally equivalent to TEP). Migrating phytoplankton can

739   clearly provide a mechanistic linkage via upward nutrient transport to the observed NO

740   anomalies.

741   **Contributions to carbon and phosphorus budgets**

742   *DIC* – Vertically migrating phytoplankton can also help explain the observed

743   summertime DIC drawdown (Gruber et al., 1998; Keeling et al., 2004) in the absence of

744   measurable nitrate from the mixed layer at both the ALOHA and BATS stations. The

745   concurrently operating migration cycles of different individuals would continually bring

746   intracellular nitrate-rich migrators into the surface mixed layer where their oxygenic

747   photosynthesis would draw down DIC and release dissolved O$_2$, contributing to rPPN anomaly

748   formation within the mixed layer. High intracellular nitrate gradients within migrators (mM to

749   nM across cell membranes) can also lead to excretion of dissolved nitrate into the water column

750   (Singler and Villareal, 2005). Thus, nitrate leakage from migrators could help explain the

751   observation of a presumed subsurface nitrate source supporting pico-eukaryotic phytoplankton in

752   the mixed layer, even during the stratified summer months at the BATS station (Fawcett et al.,

753   2011). However, nitrogen derived from migrator-mediated nitrate excretion is required to sink

754 out of the mixed layer in some form in order to contribute to summertime net DIC drawdown at

755 these two sites. Regardless of how nitrate is acquired and internally reduced (by migrators or by

756 release and uptake by non-migrating phytoplankton), it will contribute to the observed rPPN.

757   We can compare our estimated rates of rPPN formation within the euphotic zone with the

758 summertime mixed layer DIC drawdown at each time-series site using assumptions on the

759 appropriate O_2:C:N stoichiometry of production. Although seasonal rPPN formation exhibits the

760 largest increase in $preNO_3$ concentrations at ~50 – 100 m depth, seasonal accumulation of

761 residual positive $preNO_3$ is observed within the mixed layer (~0 – 30 m) at both sites (Fig. 1, 2).

762   At station ALOHA, net community production during the six-month summer to fall

763 period represents ~40% of the 2.3 mol C m^{-2} yr^{-1} ANCP (Keeling et al., 2004), yielding a

764 summertime mixed layer DIC drawdown of ~920 mmol C m^{-2}. Our estimated rate of euphotic

765 zone rPPN formation during this same seasonal period is 33 – 81 mmol N m^{-2} (Table 1). The

766 summertime DIC drawdown can be converted to residual $preNO_3$ nitrogen equivalents using the

767 literature range in O_2:C stoichiometries of production of 1.0 – 1.6 (Paulmier et al., 2009), and the

768 DOM and POM weighted O_2:N stoichiometries of production (using the values in Table 1)

769 yielding values of 7.8 – 14.3 for the C:N of summertime new production at station ALOHA.

770 Summertime DIC drawdown converted to $preNO_3$ equivalents is 64 – 118 mmol N m^{-2}. Thus,

771 our estimated rPPN formation within the euphotic zone can potentially explain 28 – >100% of

772 the mixed layer DIC drawdown at station ALOHA.

773   The estimated rate of euphotic zone rPPN formation during summer-to-fall at the BATS

774 station is 50 – 96 mmol N m^{-2} (Table 1). Net community production during this seasonal period

775 is ~45% of the 2.3 mol C m^{-2} yr^{-1} ANCP (Gruber et al., 1998), yielding a summertime mixed

776 layer DIC drawdown of ~1035 mmol C m^{-2}. Conversion of the summertime DIC drawdown to

777   preNO$_3$ nitrogen equivalents following a similar approach as our calculation at station ALOHA

778   uses a DOM and POM weighted C:N of 7.9 – 14.8 for summertime new production at the BATS

779   station, yielding 70 – 131 mmol N m^{-2}. Thus, our estimated rPPN formation within the euphotic

780   zone can potentially explain 38 – >100% of the mixed layer DIC drawdown at the BATS station.

781   *prePO$_4$* – We also investigated for the presence of subsurface residual negative prePO$_4$

782   anomalies at the ALOHA and BATS stations. Station ALOHA does not exhibit a subsurface

783   residual negative prePO$_4$ anomaly (Fig. 3), with the exception of a small anomaly present in

784   years 2002 – 2004. There does exist a subsurface residual negative prePO$_4$ anomaly and euphotic

785   zone residual positive prePO$_4$ anomaly at the BATS station (Fig. 4), present throughout the time

786   series and monthly averaged climatology that is coincident in both seasonal timing and

787   depth/density layer location as the rNPN and rPPN anomalies (Fig. 2). Carbon to phosphorus

788   ratios exhibit their global maxima in the subtropical North Atlantic for phytoplankton biomass

789   (Martiny et al., 2013), dissolved organic matter (Letscher and Moore, 2015), and exported

790   organic matter (Teng et al., 2014). The hypothesized phosphorus limitation of this basin

791   (Ammerman et al., 2003; Moore et al., 2004) may explain the contrasting observations of the

792   presence of a residual negative prePO$_4$ anomaly at the BATS station in the North Atlantic while

793   not at station ALOHA in the North Pacific. Because of the many observations of elevated C:P

794   across organic matter pools in the North Atlantic, we tested for the theoretical value of R$_{-O2:P}$, the

795   stoichiometric ratio of O$_2$ consumed to phosphate released during the remineralization of organic

796   matter, needed to eliminate the subsurface residual negative prePO$_4$ anomaly at the BATS

797   station. This theoretical value of R$_{-O2:P}$ was found to be ~1000:1 (Fig. S10), which is ~4x higher

798   than the inferred R$_{-O2:P}$ for the North Atlantic from an inversion of subsurface O$_2$ and phosphate

799   data (DeVries and Deutsch, 2014).

800   We hypothesize that P-limited or P-stressed vertically migrating phytoplankton also take

801   up phosphate at the nutricline in combination with nitrate to contribute to both the observed

802   rNPN/rPPN and the subsurface residual negative $prePO_4$ anomaly present at the BATS station.

803   Limited sampling in the waters between Hawaii and California indicated N:P ratios were not

804   significantly different between sinking and ascending *Rhizosolenia* mats (N:P ~26-30) while C:P

805   ratios were significantly different ($p = 0.05$, C:P sinkers $= 388 \pm 66$; C:P ascending $= 221 \pm 43$).

806   This is consistent with simultaneous uptake of N and P at depth, but carbon consumption at

807   depth relative to the surface. Further data on phosphate composition of vertically migrating

808   phytoplankton are needed to confirm our hypothesis.

809

810   **Concluding Remarks**

811   Subsurface residual $preNO_3$ anomalies cover a large portion of the subtropical ocean

812   (Fig. 5). Our analyses have confirmed and emphasized that the Abell et al. (2005) use of non-

813   Redfield DOM stoichiometry in the calculation of $preNO_3$ is required, and an explicit derivation

814   of r_{DOM} is needed. The residual $preNO_3$ calculation revealed a subsurface rNPN anomaly that is

815   not accounted for by organic material remineralization. Our consideration of three possible

816   contributing biological mechanisms suggest that the dominant role (in decreasing order of

817   importance) is played by vertically migrating giant phytoplankton, vertically separated TEP

818   formation and remineralization, and bacterial utilization of nitrate (Table 2). Basin-specific

819   differences in the budgets are evident with TEP appearing to be more important at station

820   ALOHA than at BATS. The analyses also revealed a near-surface rPPN anomaly that is

821   approximately balanced and concurrent with the rNPN anomaly. This feature is coherent with the

822   subsurface oxygen maximum (SOM) and we interpret this as evidence that the "missing" nitrate

823   from the rNPN anomaly is mechanistically linked to the SOM. The seasonal euphotic zone rPPN

824   anomaly can also explain a significant fraction of the unexplained summertime drawdown of

825   DIC from the mixed layer at both sites. Whether this phenomenon is predominately carried out

826   by TEP production and export, vertically migrating phytoplankton, or a combination of both

827   awaits more detailed and direct field observations. More observations of upper ocean, surface to

828   ~200 m, abundance estimates of the vertically migrating phytoplankton taxa, their intracellular

829   nitrate and phosphate contents, and their migration timescales are needed to confirm the

830   hypothesis by multiple authors (e.g. Cullen, 1985; Richardson et al., 1998; Fraga, 2001; Villareal

831   et al., 2014) of this flora's important role in nutrient transport and rNPN/rPPN anomaly

832   formation at the time-series stations (this study). Given the circumglobal, warm-water range of

833   this oligotrophic flora (Fig. S11-S13), it is reasonable to expect upward nutrient transport

834   throughout the subtropical gyres. Nitrogen-fixation may locally play a role in modifying rPPN,

835   although Johnson et al.'s (2010) budgets suggested additional nitrate-based production was

836   required. TEP may contribute as well, depending on the stoichiometry of

837   production/remineralization and shifts in buoyancy characteristics. More information on the

838   mass quantities of the positively and negatively buoyant TEP within the euphotic zone and its

839   C:N content is needed to better constrain the role of this mechanism in rPPN/rNPN anomaly

840   formation in the subtropics. In addition, *Rhizosolenia* mats are embedded in a TEP matrix

841   (Pilskaln et al., 2005), so it is likely that all three biological mechanisms we investigated are non-

842   mutually exclusive with vertically migrating phytoplankton contributing to TEP

843   production/export, nitrate transport across the nitracline into the euphotic zone, and bacterial

844   nitrate uptake to remineralize N-deficient TEP. While phytoplankton TEP production appears to

845   be favored in the upper water column, positively buoyant TEP production/formation in the

846 nutricline could also serve to provide a means for transporting entrained particulates upward into

847 the euphotic zone. Both migration and TEP are difficult to measure and the challenge will be to

848 develop methods and time-series to record these biologically driven processes at the requisite

849 time and space scales.

850

851

852

860

861 **References**

862 Abell, J., Emerson, S., and Keil, R. G.: Using preformed nitrate to infer decadal changes in DOM
863 remineralization in the subtropical North Pacific, Global Biogeochemical Cycles, 19(1), 2005.
864
865 Abell, J., Emerson, S., and Renaud, P.: Distributions of TOP, TON and TOC in the North Pacific
866 subtropical gyre: Implications for nutrient supply in the surface ocean and remineralization in the
867 upper thermocline, Journal of Marine Research, 58(2), 203-222, 2000.
868
869 Ascani F, Richards KJ, Firing E, Grant S, Johnson KS, Jia Y, Lukas R, and Karl DM.: Physical and
870 biological controls of nitrate concentrations in the upper subtropical North Pacific Ocean. Deep Sea
871 Research Part II-Topical Studies in Oceanography 93: 119-134, 2013.
872
873 Alldredge, A. L., Passow, U., and Logan, B. E.: The abundance and significance of a class of
874 large, transparent organic particles in the ocean, Deep Sea Research Part I: Oceanographic
875 Research Papers, 40(6), 1131-1140, 1993.

876

877 Alldredge, A. L., and Silver, M. W.: Abundance and production rates of floating diatom mats
878 (*Rhizosolenia castracanei* and *Rhizosolenia imbricata* var. *shrubsolei*) in the eastern Pacific
879 Ocean., Mar. Biol., 66, 83-88, 1982.

880

881 Ammerman, J. W., Hood, R. R., Case, D. A., and Cotner, J. B.: Phosphorus deficiency in the
882 Atlantic: An emerging paradigm in oceanography, Eos, Transactions American Geophysical
883 Union, 84(18), 165-170, 2003.

884

885 Anderson, L. A.: On the hydrogen and oxygen content of marine phytoplankton, Deep Sea
886 Research Part 1: Oceanographic Research Papers, 42(9), 1675-1680, 1995.

887

888 Anderson, L. A., and Sarmiento, J. L.: Redfield ratios of remineralization determined by nutrient
889 data analysis, Global Biogeochemical Cycles, 8(1), 65-80, 1994.

890

891 Azetsu-Scott, K., and Passow, U.: Ascending marine particles: Significance of transparent exopolymer
892 particles (TEP) in the upper ocean, Limnol. Oceanogr., 49, 741-748, 2004.

893

894 Ballek, R. W., and Swift, E.: Nutrient-and light-mediated buoyancy control of the oceanic non-
895 motile dinoflagellate *Pyrocystis noctiluca* Murray ex Haeckel (1890), Journal of Experimental
896 Marine Biology and Ecology, 101(1-2), 175-192, 1986.

897

898 Bauerfeind, E.: Primary production and phytoplankton biomass in the equatorial region of the
899 Atlantic at 22° west, Oceanological Acta, Proceedings of the International Symposium on
900 Equatorial Vertical Motion, 131-136, 1987.

901

902 Belyayeva, T. V.: Abundance of *Ethmodiscus* in Pacific plankton, Oceanology, Academy of
903 Science, USSR, 10, 672-675 (Translation by the American Geophysical Union), 1970.

904

905 Belyayeva, T. V.: Range and numbers of diatoms in the genus *Ethmodiscus* Castr. in the Pacific
906 plankton and sediments, Oceanology, Academy of Science, USSR, 8, 79-85, (Translation by
907 the American Geophysical Union), 1968.

908

909 Booth, B. C.: Vernal phytoplankton community in the eastern subarctic Pacific: Predominant
910 species, in: Sixth International Symposium on Fossil and Living Diatoms, edited by: Simonsen,
911 R., 339-358, 1980.

912

913 Broecker, W. S.: "NO" A conservative water-mass tracer, Earth Planet. Sci. Lett., 23, 100-107,
914 1974.

915

916 Carlson, C. A., Ducklow, H. W., and Sleeter, T. D.: Stocks and dynamics of bacterioplankton in
917 the northwestern Sargasso Sea, Deep Sea Research Part II: Topical Studies in
918 Oceanography, 43(2-3), 491-515, 1996.

919

920 Caron, D. A., Lim, E. L., Sanders, R. W., Dennett, M. R., and Berninger, U. G.: Responses of
921 bacterioplankton and phytoplankton to organic carbon and inorganic nutrient addition in two
922 oceanic ecosystems, Aquatic Microbial Ecology, 22, 175-184, 2000.
923
924 Carpenter, E. J., Harbison, R. G., Madin, L. P., Swanberg, N. R., Biggs, D. C., Hulburt, E. M.,
925 McAlister, V. L., and McCarthy, J. J.: *Rhizosolenia* Mats, Limnol. Oceanogr., 22, 739-741, 1977.
926
927 Church, M. J., Ducklow, H. W., and Karl, D. M.: Light dependence of [3H] leucine
928 incorporation in the oligotrophic North Pacific Ocean, Applied and Environmental
929 Microbiology, 70(7), 4079-4087, 2004.
930
931 Cisternas-Novoa, C., Lee, C., and Engel, A.: Transparent exopolymer particles (TEP) and
932 Coomassie stainable particles (CSP): Differences between their origin and vertical distributions
933 in the ocean, Marine Chemistry, 175, 56-71, 2015.
934
935 Cleve, P.: Seasonal distribution of Atlantic plankton organisms., D. R. Bonniers, Göteborg,
936 1900. 368 pages
937
938 Cotner, J. B., Ammerman, J. W., Peele, E. R., and Bentzen, E.: Phosphorus-limited
939 bacterioplankton growth in the Sargasso Sea, Aquatic Microbial Ecology, 13(2), 141-149, 1997.
940
941 Cowen, J. P., and Holloway, C. F.: Structural and chemical analysis of marine aggregates: in-
942 situ macrophotography and laser confocal and electron microscopy, Marine Biology (Berlin),
943 126, 163-174, 1996.
944
945 Cullen, J. J.: Diel vertical migration by dinoflagellates: roles of carbohydrate metabolism and behavioral
946 flexibility, in: Migration: mechanisms and adaptive significance, edited by: Rankin, M. A., Marine
947 Science Institute, Port Aransas, 135-152, 1985.
948
949 Darwin, C.: The Voyage of the Beagle, Natural History Library edition (1962), edited by: Engle,
950 L., Doubleday, New York, 524 pp., 1860.
951
952 DeVries, T., and Deutsch, C.: Large-scale variations in the stoichiometry of marine organic
953 matter respiration, Nature Geoscience, 7(12), 890, 2014.
954
955 Doney, S. C. and Bullister, J. L.: A chlorofluorocarbon section in the eastern North Atlantic,
956 Deep Sea Research I, 39(11-12A), 1857-1883, 1992.
957
958 Emerson, S.: Annual net community production and the biological carbon flux in the
959 ocean, Global Biogeochemical Cycles, 28(1), 14-28, 2014.
960
961 Emerson, S., Quay, P., Karl, D., Winn, C., Tupas, L., and Landry, M.: Experimental
962 determination of the organic carbon flux from open-ocean surface waters, Nature, 389(6654),
963 951, 1997.
964

965 Engel, A.: Distribution of transparent exopolymer particles (TEP) in the northeast Atlantic Ocean
966 and their potential significance for aggregation processes, Deep Sea Research Part I:
967 Oceanographic Research Papers, 51(1), 83-92, 2004.
968
969 Eppley, R. W., Holm-Hansen, O., and Strickland, J. D. H.: Some observations on the vertical migration
970 of dinoflagellates, J. Phycol., 4, 333-340, 1968.
971
972 Fawcett, S. E., Lomas, M. W., Casey, J. R., Ward, B. B., and Sigman, D. M.: Assimilation of
973 upwelled nitrate by small eukaryotes in the Sargasso Sea, Nature Geoscience, 4(10), 717, 2011.
974
975 Fraga, F.: Phytoplanktonic biomass synthesis: application to deviations from Redfield
976 stoichiometry, Sci. Mar., 65, 153-169, 2001.
977
978 Fraga, F., Pérez, F. F., Figueiras, F. G., and Rios, A. F.: Stoichiometric variations of N, P, C and
979 O_2 during a *Gymnodinium catenatum* red tide and their interpretation, Mar. Ecol. Prog. Ser., 87,
980 123-134, 1992.
981
982 Fraga, F., Rios, A. F., Pérez, F. F., Estrada, M., and Marrase, C.: Effect of upwelling pulses on
983 excess carbohydrate synthesis as deduced from nutrient, carbon dioxide, and oxygen profiles,
984 Mar. Ecol. Prog. Ser., 189, 65-75, 1999.
985
986 Ganf, G. G., and Oliver, R. L.: Vertical separation of light and available nutrients as a factor
987 causing replacement of green algae by blue-green algae in the plankton of a stratified lake, The
988 Journal of Ecology, 829-844, 1982.
989
990 Garcia, H. E., Locarnini, R. A., Boyer, T. P., Antonov, J. I., Baranova, O. K., Zweng, M. M.,
991 Reagan, J. R., Johnson, D. R.: World Ocean Atlas 2013, Volume 3: Dissolved Oxygen, Apparent
992 Oxygen Utilization, and Oxygen Saturation, S. Levitus, Ed., A. Mishonov Technical Ed., NOAA
993 Atlas NESDIS 75, 27, 2014a.
994
995 Garcia, H. E., Locarnini, R. A., Boyer, T. P., Antonov, J. I., Baranova, O. K., Zweng, M. M.,
996 Reagan, J. R., Johnson, D. R.: World Ocean Atlas 2013, Volume 4: Dissolved Inorganic
997 Nutrients (phosphate, nitrate, silicate), S. Levitus, Ed., A. Mishonov Technical Ed., NOAA Atlas
998 NESDIS 76, 25, 2014b.
999
1000 Goncalves da Silva, M. G.: Diatom (Bacillariophyceae) distribution in the continental shelf of
1001 Pernambuco (Brazil).), Trab. Oceanogr. Univ. Fed. Pernambuco., 17, 7-46 (in Spanish), 1982.
1002
1003 Gruber, N., Keeling, C. D., and Bates, N. R.: Interannual variability in the North Atlantic Ocean
1004 carbon sink, Science, 298(5602), 2374-2378, 2002.
1005
1006 Gruber, N., Keeling, C. D., and Stocker, T. F.: Carbon-13 constraints on the seasonal inorganic
1007 carbon budget at the BATS site in the northwestern Sargasso Sea, Deep Sea Research Part I:
1008 Oceanographic Research Papers, 45(4-5), 673-717, 1998.
1009

1010 Guidi, L., Calil, P. H. R., Duhamel, S., Bjoerkman, K. M., Doney, S. C., Jackson, G. A., Li, B., Church,
1011 M. J., Tozzi, S., Kolber, Z. S., Richards, K. J., Fong, A. A., Letelier, R. M., Gorsky, G., Stemmann, L.,
1012 and Karl, D. M.: Does eddy-eddy interaction control surface phytoplankton distribution and carbon
1013 export in the North Pacific Subtropical Gyre?, J. Geophys. Res.-Biogeosci., 117,
1014 10.1029/2012jg001984, 2012.
1015
1016 Gundersen, K., Heldal, M., Norland, S., Purdie, D. A., and Knap, A. H.: Elemental C, N, and P
1017 cell content of individual bacteria collected at the Bermuda Atlantic Time-series Study (BATS)
1018 site, Limnology and Oceanography, 47(5), 1525-1530, 2002.
1019
1020 Hamanaka, J., Tanoue, E., Hama, T., and Handa, N.: Production and export of particulate fatty
1021 acids, carbohydrates and combined amino acids in the euphotic zone, Marine Chemistry, 77(1),
1022 55-69, 2002.
1023
1024 Hansell, D. A., and Carlson, C. A.: Biogeochemistry of total organic carbon and nitrogen in the
1025 Sargasso Sea: control by convective overturn, Deep Sea Research Part II: Topical Studies in
1026 Oceanography, 48(8), 1649-1667, 2001.
1027
1028 Hasle, G. R.: Phototactic vertical migration in marine dinoflagellates, Oikos, 2(2), 162-175,
1029 1950.
1030
1031 Jenkins, W. J., and Doney, S. C.: The subtropical nutrient spiral, Global Biogeochemical
1032 Cycles, 17(4), 2003.
1033
1034 Jenkins, W. J., and Goldman, J. C.: Seasonal oxygen cycling and primary production in the
1035 Sargasso Sea, Journal of Marine Research, 43(2), 465-491, 1985.
1036
1037 Johnson, K. S., Riser, S. C., and Karl, D. M.: Nitrate supply from deep to near-surface waters of
1038 the North Pacific subtropical gyre, Nature, 465(7301), 1062, 2010.
1039
1040 Joseph, L., Villareal, T. A., and Lipschultz, F.: A high sensitivity nitrate reductase assay and its
1041 application to vertically migrating Rhizosolenia mats, Aquatic Microbial Ecology, 12(1), 95-104,
1042 1997.
1043
1044 Kahn, H., and Swift, E.: Positive buoyancy through ionic control in the nonmotile marine
1045 dinoflagellate *Pyrocystis noctiluca* Murray ex Schuett, Limnology and Oceanography, 23, 649-
1046 658, 1978.
1047
1048 Keeling, C. D., Brix, H., and Gruber, N.: Seasonal and long-term dynamics of the upper ocean
1049 carbon cycle at Station ALOHA near Hawaii, Global Biogeochemical Cycles, 18(4), 2004.
1050
1051 Kirchman, D. L.: The uptake of inorganic nutrients by heterotrophic bacteria, Microbial
1052 Ecology, 28(2), 255-271, 1994.
1053

1054   Letscher, R. T., Knapp, A. N., James, A. K., Carlson, C. A., Santoro, A. E., and Hansell, D. A.:
1055   Microbial community composition and nitrogen availability influence DOC remineralization in
1056   the South Pacific Gyre, Marine Chemistry, 177, 325-334, 2015.
1057
1058   Letscher, R. T., and Moore, J. K.: Preferential remineralization of dissolved organic phosphorus
1059   and non-Redfield DOM dynamics in the global ocean: Impacts on marine productivity, nitrogen
1060   fixation, and carbon export, Global Biogeochemical Cycles, 29(3), 325-340, 2015.
1061
1062   Letscher, R. T., Primeau, F., and Moore, J. K.: Nutrient budgets in the subtropical ocean gyres
1063   dominated by lateral transport, Nature Geoscience, 9(11), 815-819, 2016.
1064
1065   Long, R. A., and Azam, F.: Abundant protein-containing particles in the sea, Aquatic Microbial
1066   Ecology, 10, 213, 1996.
1067
1068   Mari, X., Passow, U., Migon, C., Burd, A. B., and Legendre, L.: Transparent exopolymer
1069   particles: Effects on carbon cycling in the ocean, Progress in Oceanography, 151, 13-37, 2017.
1070
1071   Martin, J. H., Knauer, G. A., Karl, D. M., and Broenkow, W. W.: VERTEX: carbon cycling in
1072   the northeast Pacific. Deep Sea Research Part A, Oceanographic Research Papers, 34(2), 267-
1073   285, 1987.
1074
1075   Martinez, L. A.: Nitrogen fixation by floating diatom mats: a source of new nitrogen to
1076   oligotrophic ocean waters, Biology, University of California, Santa Cruz, 23 pp., 1982.
1077
1078   Martiny, A. C., Pham, C. T., Primeau, F. W., Vrugt, J. A., Moore, J. K., Levin, S. A., and Lomas,
1079   M. W.: Strong latitudinal patterns in the elemental ratios of marine plankton and organic
1080   matter, Nature Geoscience, 6(4), 279, 2013.
1081
1082   Michaels, A. F., Bates, N. R., Buesseler, K. O., Carlson, C. A., and Knap, A. H.: Carbon-cycle
1083   imbalances in the Sargasso Sea, Nature, 372(6506), 537, 1994.
1084
1085   Mikkelsen, N.: On the origin of *Ethmodiscus* ooze, Marine Micropaleontology, 2, 35-46,
1086   10.1016/0377-8398(77)90004-4, 1977.
1087
1088   Moore, J. K., Doney, S. C., and Lindsay, K.: Upper ocean ecosystem dynamics and iron cycling
1089   in a global three-dimensional model, Global Biogeochemical Cycles, 18(4), 2004.
1090
1091   Moore, J. K., and Villareal, T. A.: Size-ascent rate relationships in positively buoyant marine
1092   diatoms, Limnology and Oceanography, 41(7), 1514-1520, 1996.
1093
1094   Navarro, G., and Ruiz, J.: Hysteresis conditions the vertical position of deep chlorophyll
1095   maximum in the temperate ocean, Global Biogeochemical Cycles, 27(4), 1013-1022, 2013.
1096
1097   Olsen, A., Key, R. M., van Heuven, S., Lauvset, S.K., Velo, A., Lin, X., Schirnick, C., Kozyr,
1098   A., Tanhua, T., Hoppema, M., Jutterström, S., Steinfeldt, R., Jeansson, E., Ishii, M., Pérez, F.F.,

1099 and Suzuki, T.: The Global Ocean Data Analysis Project version 2 (GLODAPv2) - an internally
1100 consistent data product for the world ocean, Earth System Science Data, 8, 297-323, 2016.

1102 Paulmier, A., Kriest, I., and Oschlies, A.: Stoichiometries of remineralisation and denitrification
1103 in global biogeochemical ocean models, Biogeosciences, 6(5), 923-935, 2009.

1105 Pilskaln, C. H., Villareal, T. A., Dennett, M., Darkangelo-Wood, C., and Meadows, G.: High
1106 concentrations of marine snow and diatom algal mats in the North Pacific Subtropical Gyre:
1107 Implications for carbon and nitrogen cycles in the oligotrophic ocean, Deep Sea Research Part I:
1108 Oceanographic Research Papers, 52(12), 2315-2332, 2005.

1110 Platt, T., Harrison, W. G., Lewis, M. R., Li, W. K., Sathyendranath, S., Smith, R. E., and Vezina,
1111 A. F.: Biological production of the oceans: the case for a consensus, Marine Ecology Progress
1112 Series, 77-88, 1989.

1114 Ricard, M.: Observations sur les diatomées marines du genre *Ethmodiscus* Castr., Rev. Algol.
1115 N.S.O, 10, 56-73, 1970.

1117 Richardson, T. L., Ciotti, A. M., Cullen, J. J., and Villareal, T. A.: Physiological and optical
1118 properties of *Rhizosolenia formosa* (Bacillariophyceae) in the context of open-ocean vertical
1119 migration, Journal of Phycology, 32(5), 741-757, 1996.

1121 Richardson, T. L., Cullen, J. J., Kelley, D. E., and Lewis, M. R.: Potential contributions of
1122 vertically migrating Rhizosolenia to nutrient cycling and new production in the open
1123 ocean, Journal of Plankton Research, 20(2), 219-241, 1998.

1125 Ricker, W. E.: Linear regressions in fishery research, Journal of the fisheries board of
1126 Canada, 30(3), 409-434, 1973.

1128 Rivkin, R. B., and Anderson, M. R.: Inorganic nutrient limitation of oceanic
1129 bacterioplankton, Limnology and Oceanography, 42(4), 730-740, 1997.

1131 Rivkin, R. B., Swift, E., Biggley, W. H., and Voytek, M. A.: Growth and carbon uptake by
1132 natural populations of oceanic dinoflagellates *Pyrocystis noctiluca* and *Pyrocystis*
1133 *fusiformis*, Deep Sea Research Part A. Oceanographic Research Papers, 31(4), 353-367, 1984.

1135 Semina, H. J., and Levashova, S. S.: The biogeography of tropical phytoplankton species in the
1136 Pacific Ocean, Int. Rev. Gesamten Hydrobiol., 78, 243-262, 1993.

1138 Semina, H. J., Belyayeva, T. V., Zernova, V. V., MovChan, O. A., Sanina, L. V., Sukhanova, I.
1139 N., and Tarkhova, I. A.: Distribution of indicator species of planktonic algae in the World Ocean,
1140 Oceanology, 17, 573-579, 1977.

1142 Shipe, R. F., Brzezinski, M. A., Pilskaln, C., and Villareal, T. A.: *Rhizosolenia* mats: An
1143 overlooked source of silica production in the open sea., Limnology and Oceanography, 44, 1282-
1144 1292, 1999.

1145

1146 Shulenberger, E., and Reid, J. L.: The Pacific shallow oxygen maximum, deep chlorophyll
1147 maximum, and primary productivity, reconsidered, Deep Sea Research Part A. Oceanographic
1148 Research Papers, 28(9), 901-919, 1981.

1149

1150 Singler, H. R., and Villareal, T. A.: Nitrogen inputs into the euphotic zone by vertically
1151 migrating *Rhizosolenia* mats, Journal of Plankton Research, 27(6), 545-556, 2005.

1152

1153 Steemann Nielsen, E.: Über die vertikale Verbreitung der Phytoplanktonten im Meere, Internationale
1154 Revue der gesamten Hydrobiologie und Hydrographie, 38, 421-440, 10.1002/iroh.19390380124, 1939.

1155

1156 Sukhanova, I. N., and Rudyakov, Y. A.: Population composition and vertical distribution of
1157 *Pyrocystis pseudonoctiluca* (W. Thomson) in the western equatorial Pacific, in: Life activities of
1158 pelagic communities in the ocean., edited by: Vinogradov, M. E., Israeli Program Scientific
1159 Translation. Jerusalem., 218-228, 1973.

1160

1161 Sukhanova, V. N.: Vertical distribution of some peridinians in the equatorial Pacific Ocean, in:
1162 Life activities of pelagic communities in the ocean., edited by: Vinogradov, M. E., Israeli
1163 Program Scientific Translation. Jerusalem., 210-217, 1973.

1164

1165 Swift, E.: The marine diatom *Ethmodiscus rex*: its morphology and occurrence in the plankton of
1166 the Sargasso Sea, J. Phycol., 2, 456-460, 1973.

1167

1168 Swift, E., Biggley, W. H., and Seliger, H. H.: Species of oceanic dinoflagellates in genera
1169 *Dissodinium* and *Pyrocystis*: Interclonal and interspecific comparisons of coloar and photon
1170 yield of bioluminscence, Journal of Phycology, 9, 420-426, 10.1111/j.0022-3646.1973.00420.x,
1171 1973.

1172

1173 Swift, E., Meunier, V. A., Biggley, W. H., Hoarau, J., and Barras, H.: Factors affecting
1174 bioluminescence capacity in oceanic dinoflagellates, in: Bioluminescence: current perspectives,
1175 edited by: Nealson, K. H., Burgess Publishing Co., Minneapolis, 95-106, 1981.

1176

1177 Swift, E., Stuart, M., and Meunier, V.: The *in situ* growth rates of some deep-living oceanic
1178 dinoflagellates: *Pyrocystis fusiformis* and *Pyrocystis noctiluca*, Limnology and Oceanography,
1179 21, 418-426, 1976.

1180

1181 Takahashi, T., Broecker, W. S., and Langer, S.: Redfield ratio based on chemical data from
1182 isopycnal surfaces, Journal of Geophysical Research: Oceans, 90(C4), 6907-6924, 1985.

1183

1184 Teng, Y. C., Primeau, F. W., Moore, J. K., Lomas, M. W., and Martiny, A. C.: Global-scale
1185 variations of the ratios of carbon to phosphorus in exported marine organic matter, Nature
1186 Geoscience, 7(12), 895, 2014.

1187

1188 Toggweiler, J. R.: Carbon overconsumption, Nature, 363(6426), 210, 1993.

1189

1190 Toggweiler, J. R.: Vanishing in Bermuda, Nature, 372(6506), 505, 1994.

1191

1192 Trujillo-Ortiz, A. and Hernandez-Walls, R.: gmregress: Geometric Mean Regression (Reduced
1193 Major Axis Regression), A MATLAB file, http://www.mathworks.com/matlabcentral/
1194 fileexchange/27918-gmregress, 2010.

1195

1196 Venrick, E. L.: The distribution and ecology of oceanic diatoms in the North Pacific, Ph.D.,
1197 University of California, San Diego. 684 pp., 1969.

1198

1199 Villareal, T. A.: Abundance of the giant diatom *Ethmodiscus* in the southwest Atlantic Ocean
1200 and central Pacific gyre, Diatom Research, 8, 171-177, 1993.

1201

1202 Villareal, T. A.: Single-cell pulse amplitude modulation fluorescence measurements of the giant
1203 diatom Ethmodiscus (Bacillariophyceae), Journal of Phycology, 40, 1052-1061, 10.1111/j.1529-
1204 8817.2004.03208.x, 2004.

1205

1206 Villareal, T. A., Altabet, M. A., and Culver-Rymsza, K.: Nitrogen transport by vertically
1207 migrating diatom mats in the North Pacific Ocean, Nature, 363(6431), 709, 1993.

1208

1209 Villareal, T. A., and Carpenter, E. J.: Chemical composition and photosynthetic characteristics of
1210 *Ethmodiscus rex* (Bacillariophyceae): Evidence for vertical migration, Journal of Phycology, 30,
1211 1-8, 1994.

1212

1213 Villareal, T. A., and Carpenter, E. J.: Nitrogen-fixation, suspension characteristics and chemical
1214 composition of *Rhizosolenia* mats in the central North Pacific Gyre, Biological Oceanography, 6,
1215 327-345, 1989.

1216

1217 Villareal, T. A., Joseph, L., Brzezinski, M. A., Shipe, R. F., Lipschultz, F., and Altabet, M. A.:
1218 Biological and chemical characteristics of the giant diatom *Ethmodiscus* (Bacillariophyceae) in
1219 the central North Pacific gyre, Journal of Phycology, 35, 896-902, 1999a.

1220

1221 Villareal, T. A., and Lipschultz, F.: Internal nitrate concentrations in single cells of large
1222 phytoplankton from the Sargasso Sea, Journal of Phycology, 31(5), 689-696, 1995.

1223

1224 Villareal, T. A., McKay, R. M. L., Al-Rshaidat, M. M. D., Boyanapalli, R., and Sherrell, R. M.:
1225 Compositional and fluorescence characteristics of the giant diatom *Ethmodiscus* along a 3000 km
1226 transect (28 N) in the central North Pacific gyre, Deep Sea Research Part I: Oceanographic
1227 Research Papers, 54(8), 1273-1288, 2007.

1228

1229 Villareal, T. A., Pilskaln, C., Brzezinski, M., Lipschultz, F., Dennett, M., and Gardner, G. B.:
1230 Upward transport of oceanic nitrate by migrating diatom mats, Nature, 397, 423-425, 1999b.

1231

1232 Villareal, T. A., Pilskaln, C. H., Montoya, J. P., and Dennett, M.: Upward nitrate transport by
1233 phytoplankton in oceanic waters: balancing nutrient budgets in oligotrophic seas, PeerJ, 2, e302,
1234 2014.

1235

1236 Villareal, T. A., Woods, S., Moore, J. K., and Culver-Rymsza, K.: Vertical migration of
1237 Rhizosolenia mats and their significance to NO3− fluxes in the central North Pacific
1238 gyre, Journal of Plankton Research, 18(7), 1103-1121, 1996.
1239
1240 Walker, S. J., Weiss, R. F., and Salameh, P. K.: Reconstructed histories of the annual mean
1241 atmospheric mole fractions for the halocarbons CFC-11, CFC-12, CFC-113, and carbon
1242 tetrachloride, Journal of Geophysical Research-Oceans, 105(C6), 14285-14296, 2000.
1243
1244 Wallich, G. C.: On microscopic objects collected in India, & c., Transactions of the
1245 Microscopical Society of London, 6, 81-87, 1858.
1246
1247 Warner, M. J., and Weiss, R. F.: Solubilities of chlorofluorocarbons 11 and 12 in water and
1248 seawater, Deep Sea Research Part A, 32(12), 1485-1497, 1985.
1249
1250 Wiebe, P. H., Remsen, C. C., and Vaccaro, R. F.: *Halosphaera viridis* in the Mediterranean Sea:
1251 size range, vertical distribution, and potential energy source for deep-sea benthos, in Deep Sea
1252 Research and Oceanographic Abstracts (Vol. 21, No. 8, pp. 657-667), Elsevier, 1974.
1253
1254 Williams, P. J. L. B., Quay, P. D., Westberry, T. K., and Behrenfeld, M. J.: The oligotrophic
1255 ocean is autotrophic, Annual review of Marine Science, 5, 535-549, 2013.
1256
1257 Woods, S., and Villareal, T. A.: Intracellular ion concentrations and cell sap density in positively
1258 buoyant oceanic phytoplankton, Nova Hedwigia Beihefte, 133, 131, 2008.
1259
1260 Wurl, O., Miller, L., Röttgers, R., and Vagle, S.: The distribution and fate of surface-active
1261 substances in the sea-surface microlayer and water column, Marine Chemistry, 115(1-2), 1-9,
1262 2009.
1263
1264 Wurl, O., Miller, L., and Vagle, S.: Production and fate of transparent exopolymer particles in
1265 the ocean, Journal of Geophysical Research: Oceans, 116(C7), 2011.
1266
1267 Zweifel, U. L., Norrman, B., and Hagstrom, A.: Consumption of dissolved organic carbon by marine
1268 bacteria and demand for inorganic nutrients, Mar. Ecol. Prog. Ser., 101, 23-32, 1993.
1269

1270
1271
1272
1273
1274
1275
1276
1277
1278
1279
1280
1281
1282
1283

Table 1. Residual negative preNO$_3$ (rNPN) and residual positive preNO$_3$ (rPPN) anomaly

formation rates at stations ALOHA and BATS.

	Depth (m) or Neutral Density γ^n	f_{DOM}	r_{DOM}	r_{POM}	rNPN		rPPN	
					μmol N m^{-3} d^{-1}	mmol N m^{-2} yr^{-1}	μmol N m^{-3} d^{-1}	mmol N m^{-2} yr^{-1}
ALOHA	0 – 100 m	0.5	18.1	10.6	--	--	2.4 ± 0.8	43.5 ± 10.5
				6.9	--	--	3.3 ± 1.1	61.2 ± 20.2
	24.2 – 24.7	0.5	18.1	10.6	3.0 ± 1.5	17.9 ± 7.4	--	--
				6.9	2.8 ± 1.4	28.3 ± 9.6	--	--
	24.7 – 25.2	0.5	18.9	10.6	2.5 ± 1.4	13.7 ± 7.8	--	--
				6.9	1.6 ± 0.8	18.1 ± 8.8	--	--
Total	r_{POM} = 10.6				--	31.6 ± 10.8	--	--
Total	r_{POM} = 6.9				--	46.4 ± 13.0	--	--
BATS	0 – 80 m	0.4	21.1	10.6	--	--	4.1 ± 0.8	61.8 ± 12.2
				6.9	--	--	5.8 ± 1.2	82.1 ± 13.8
	25.8 – 26.3	0.4	21.1	10.6	3.8 ± 3.1	46.0 ± 39.3	--	--
				6.9	5.5 ± 2.7	87.1 ± 41.0	--	--

1301 **Table 2.** Contribution of N-poor DOM remineralization to NPN and PPN anomaly formation

1302 rates as well as contributions to rNPN and rPPN anomaly formation rates by presumed processes

1303 at the time-series sites. NPN/rNPN is for feature on $\gamma^n = 24.2 - 25.2$ at station ALOHA and $\gamma^n =$

1304 25.8 − 26.3 at the BATS station. Ez PPN/rPPN is for feature at 0 − 100 m depth at station

1305 ALOHA and 0 − 80 m depth at the BATS station.

1306

Station	preNO$_3$ Feature	N-poor DOM remineralization	Residual preNO$_3$ Feature	Proposed attributable process		
				TEP production & remineralization	Bacterial nitrate uptake	Phytoplankton vertical migration
ALOHA	NPN	1 – 16 mmol N m^{-2} yr^{-1}	rNPN	16 – 22 mmol N m^{-2} yr^{-1}	0.0 – 3.4 mmol N m^{-2} yr^{-1}	16 – 21 mmol N m^{-2} yr^{-1}
	Ez PPN	2 – 21 mmol N m^{-2} yr^{-1}	Ez rPPN	16 – 22 mmol N m^{-2} yr^{-1}	--	27 – 36 mmol N m^{-2} yr^{-1}
			% rNPN	47 – 50%	0 – 7%	45 – 50%
			% Ez rPPN	37 – 41%	--	59 – 63%
BATS	NPN	1 – 14 mmol N m^{-2} yr^{-1}	rNPN	3.2 – 6.0 mmol N m^{-2} yr^{-1}	0.2 – 3.0 mmol N m^{-2} yr^{-1}	43 – 78 mmol N m^{-2} yr^{-1}
	Ez PPN	2 – 17 mmol N m^{-2} yr^{-1}	Ez rPPN	3.2 – 6.0 mmol N m^{-2} yr^{-1}	--	59 – 76 mmol N m^{-2} yr^{-1}
			% rNPN	6 – 7%	0.5 – 3.5%	90 – 93%
			% Ez rPPN	5 – 7%	--	93 – 95%

1307

1308

1309

1310

1311

1312

1313

1314 **Figure 1.** (a) Climatology of the residual preNO$_3$ tracer [μM] in the upper 250 m at station

1315 ALOHA (22.75 °N 158 °W) for a value of r_{POM} = 10.6. Black contour lines show neutral density

1316 $γ^n$ = 24.2, 24.7, and 25.2. (b) The monthly averaged residual preNO$_3$ [μM] climatology for all
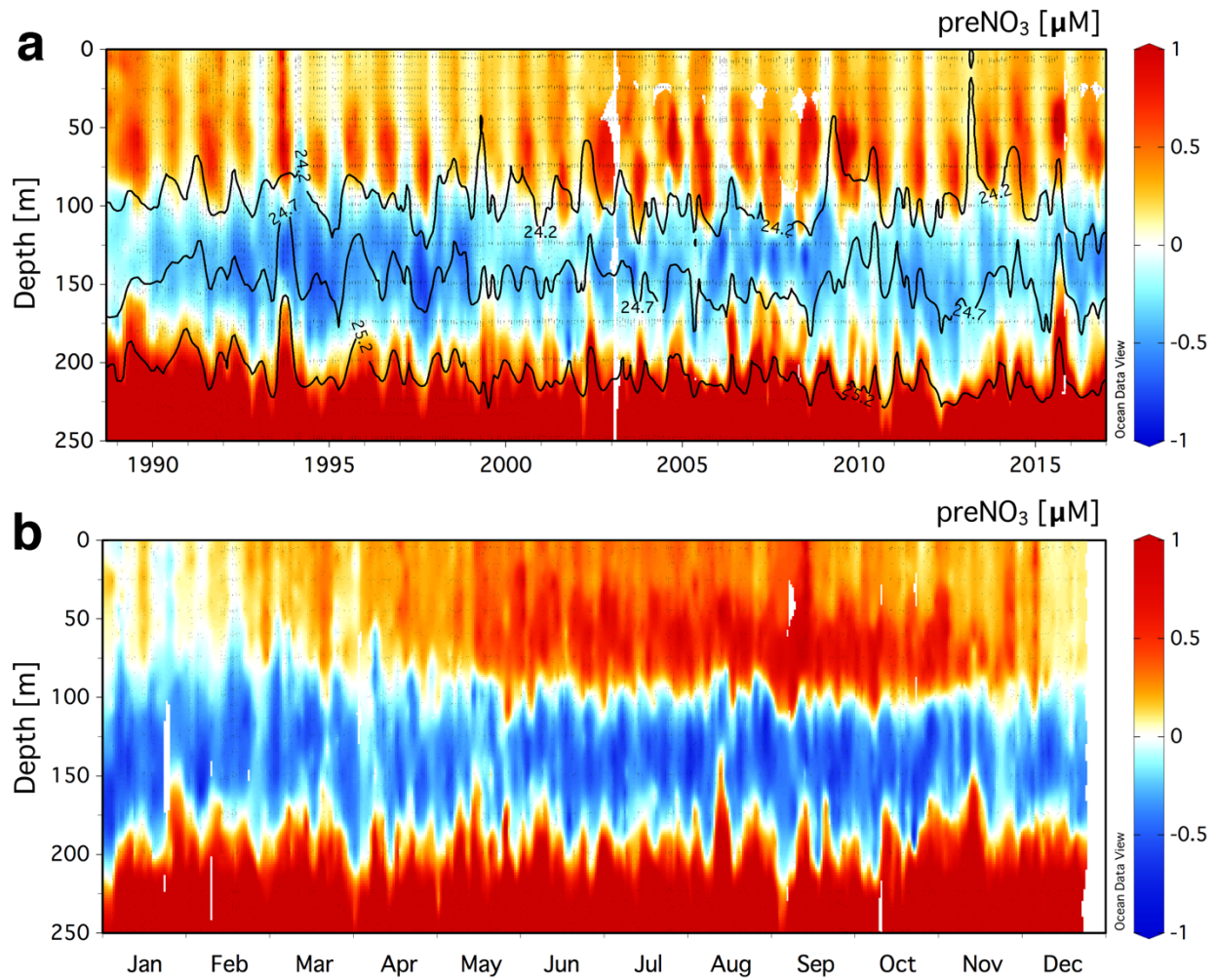
1317 data in years 1989 – 2016.

1318

1319

1320

1321

1322

1323

1324 **Figure 2.** (a) Climatology of the residual preNO$_3$ tracer [μM] in the upper 200 m at the BATS

1325 station (31.67 ºN 64.17 ºW) for a value of r_{POM} = 10.6. Black contour lines show neutral density

1326 γ^n = 25.8 and 26.3. (b) The monthly averaged residual preNO$_3$ [μM] climatology for all data in
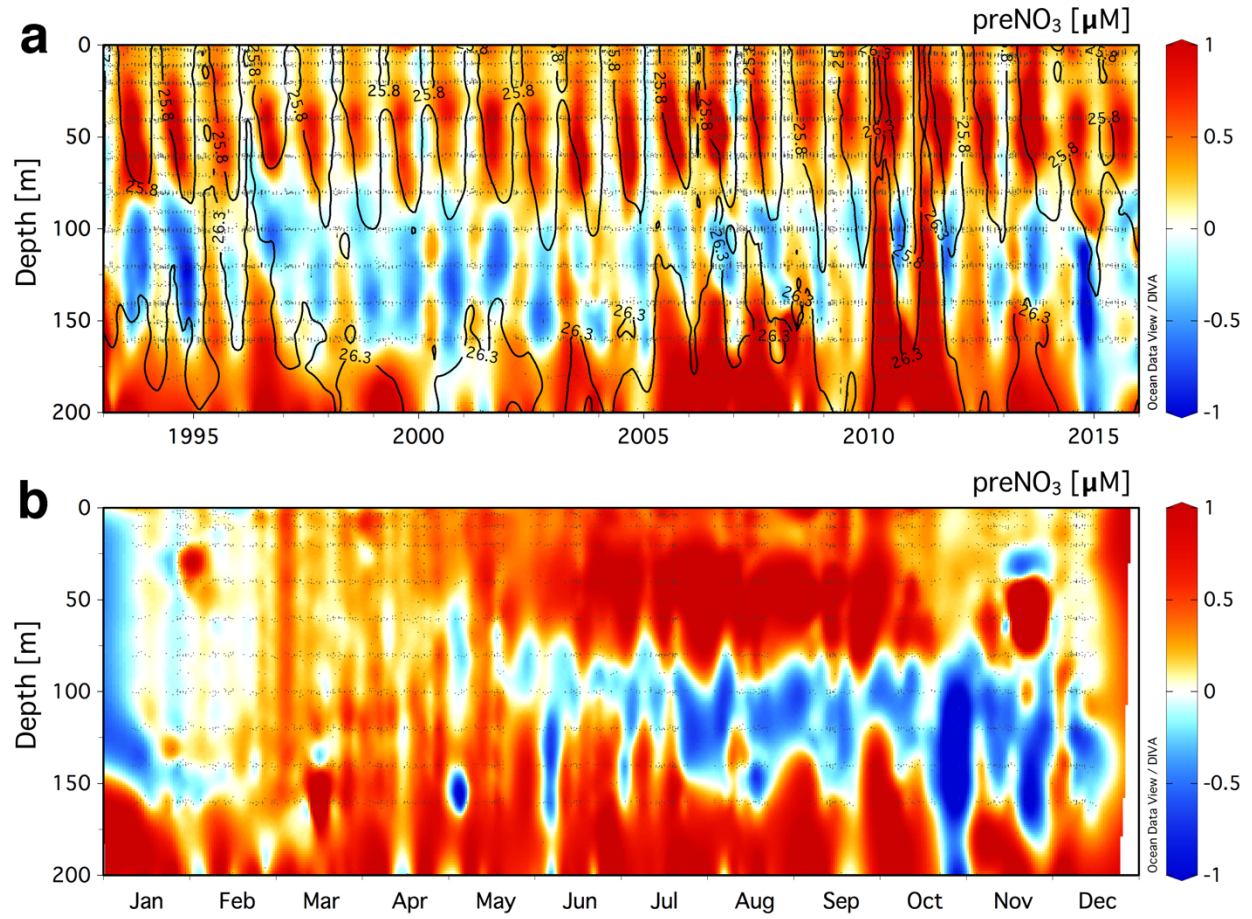
1327 years 1993 – 2016.

1328

1329

1330

1331

1332

1333

1334   **Figure 3.** (a) Climatology of the residual prePO4 tracer [μM] in the upper 250 m at station

1335   ALOHA (22.75 ºN 158 ºW) for a value of r_{POM} = 10.6. Black contour lines show neutral density

1336 γ^n = 24.2, 24.7, and 25.2. (b) The monthly averaged residual prePO4 [μM] climatology for all

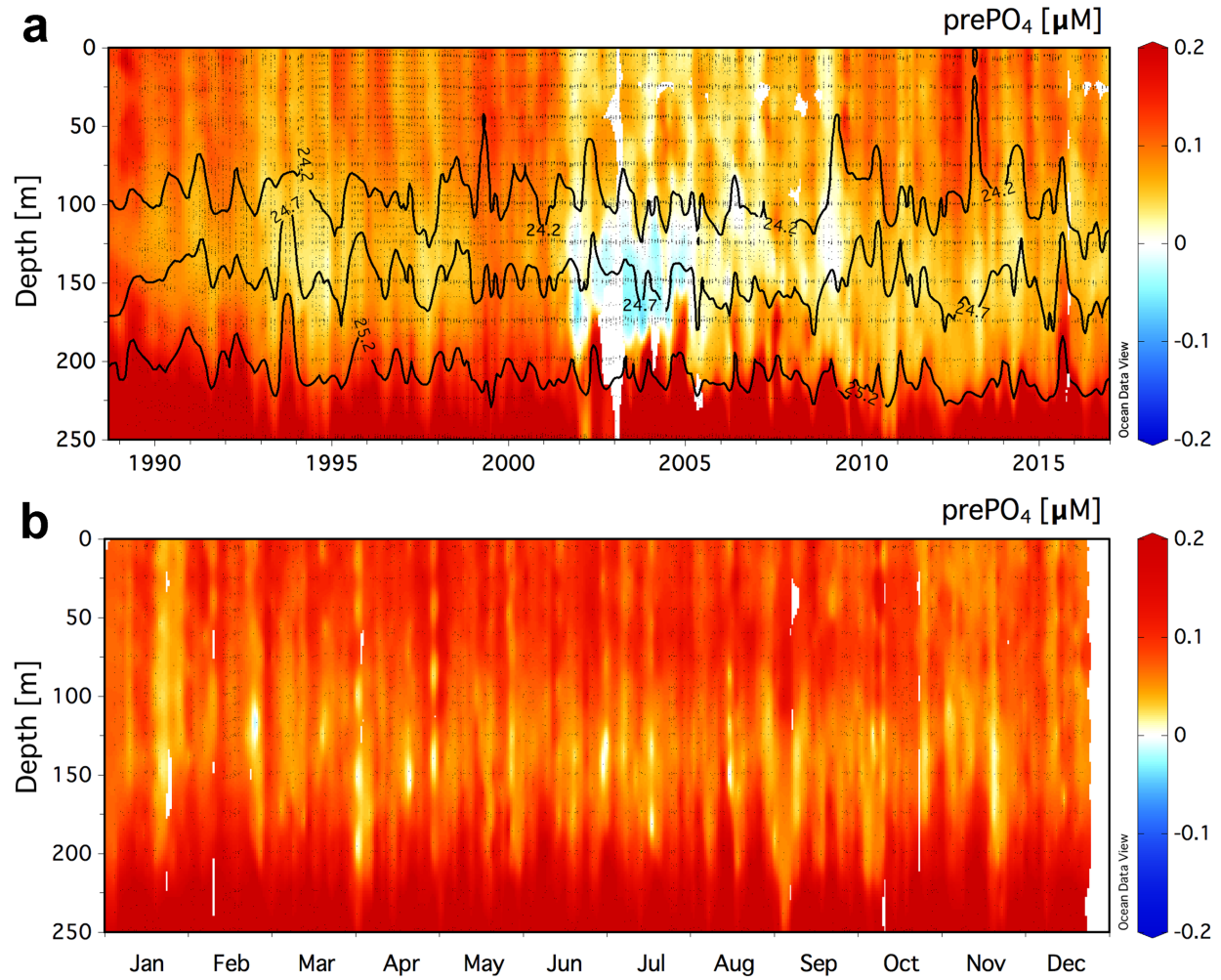1337   data in years 1989 – 2016.

1338

1339

1340

1341

1342

1343

Figure 4. (a) Climatology of the residual prePO$_4$ tracer [μM] in the upper 200 m at the BATS station (31.67 ºN 64.17 ºW) for a value of r_{POM} = 10.6. Black contour lines show neutral density γ^n = 25.8 and 26.3. (b) The monthly averaged residual prePO$_4$ [μM] climatology for all data in years 1993 – 2016.
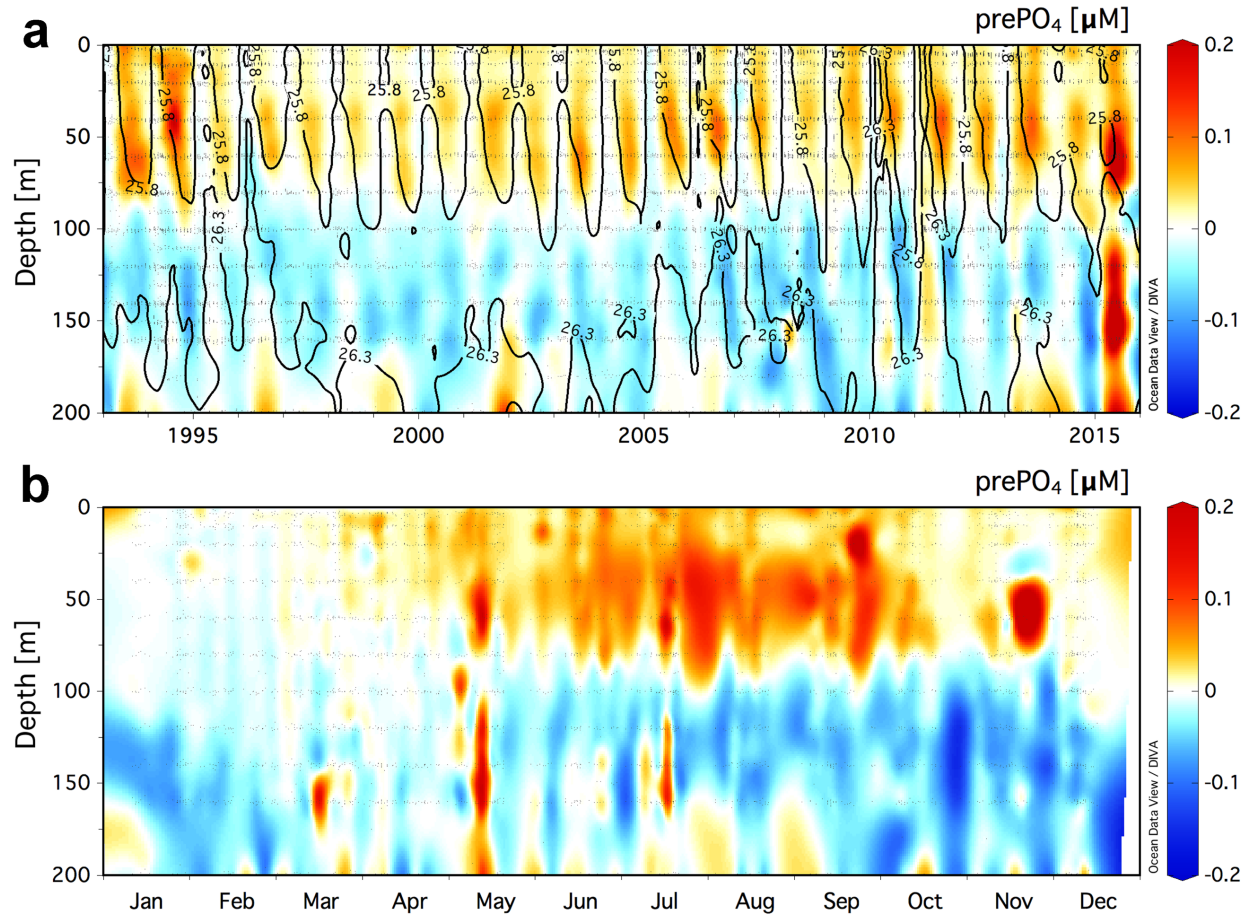
1354 **Figure 5.** Seasonal climatology of the residual preNO$_3$ tracer [μM] at 150 m depth from the

1355 World Ocean Atlas, 2013, 1° climatologies of O$_2$ anomaly and nitrate. Residual preNO$_3$ is

1356 calculated using values of $f_{DOM} = 0.5$, $r_{DOM} = 20.0$, and $r_{POM} = 8.75$.

1357

1358